

Prompt and non-prompt J/ψ production and nuclear modification at mid-rapidity in p-Pb collisions at $\sqrt{s_{NN}}=5.02$ TeV

(ALICE Collaboration) Acharya, S.; ...; Antičić, Tome; ...; Erhardt, Filip; ...; Gotovac, Sven; ...; Jerčić, Marko; ...; ...

Source / Izvornik: **European Physical Journal C, 2018, 78**

Journal article, Published version

Rad u časopisu, Objavljena verzija rada (izdavačev PDF)

<https://doi.org/10.1140/epjc/s10052-018-5881-2>

Permanent link / Trajna poveznica: <https://um.nsk.hr/um:nbn:hr:217:249684>

Rights / Prava: [Attribution 4.0 International](#)/[Imenovanje 4.0 međunarodna](#)

Download date / Datum preuzimanja: **2025-02-20**



Repository / Repozitorij:

[Repository of the Faculty of Science - University of Zagreb](#)



Prompt and non-prompt J/ψ production and nuclear modification at mid-rapidity in p–Pb collisions at $\sqrt{s_{NN}} = 5.02$ TeV

ALICE Collaboration*

CERN, 1211 Geneva 23, Switzerland

Received: 21 February 2018 / Accepted: 8 May 2018 / Published online: 8 June 2018
© CERN for the benefit of the ALICE collaboration 2018

Abstract A measurement of beauty hadron production at mid-rapidity in proton-lead collisions at a nucleon–nucleon centre-of-mass energy $\sqrt{s_{NN}} = 5.02$ TeV is presented. The semi-inclusive decay channel of beauty hadrons into J/ψ is considered, where the J/ψ mesons are reconstructed in the dielectron decay channel at mid-rapidity down to transverse momenta of 1.3 GeV/ c . The $b\bar{b}$ production cross section at mid-rapidity, $d\sigma_{b\bar{b}}/dy$, and the total cross section extrapolated over full phase space, $\sigma_{b\bar{b}}$, are obtained. This measurement is combined with results on inclusive J/ψ production to determine the prompt J/ψ cross sections. The results in p–Pb collisions are then scaled to expectations from pp collisions at the same centre-of-mass energy to derive the nuclear modification factor R_{pPb} , and compared to models to study possible nuclear modifications of the production induced by cold nuclear matter effects. R_{pPb} is found to be smaller than unity at low p_T for both J/ψ coming from beauty hadron decays and prompt J/ψ .

1 Introduction

In high-energy hadronic collisions the production of beauty-flavoured hadrons, referred to as b-hadrons (h_b) in the following, represents a challenging testing ground for models based on quantum chromodynamics (QCD).

In proton–proton (pp) collisions the production cross sections can be computed with a factorisation approach [1, 2], as a convolution of the parton distribution functions (PDFs) of the incoming protons, the partonic hard-scattering cross sections, and the fragmentation functions.

In ultra-relativistic heavy-ion collisions, where the formation of a high-density colour-deconfined medium, the quark–gluon plasma (QGP), is expected [3, 4], heavy quarks are considered as prime probes of the properties of the medium created in the collision. Indeed, they are produced in scattering processes with large momentum transfer in the first stage of

the collision and traverse the medium interacting with its constituents, thus experiencing its full evolution. Modifications in the production of b-hadrons with respect to expectations from an incoherent superposition of elementary pp collisions can reveal the properties of the medium. However, other effects, which are not related to the presence of a QGP, the so called cold nuclear matter (CNM) effects, can modify b-hadron production in heavy-ion collisions. In the initial state, the nuclear environment affects the free nucleon PDFs, which are modified depending on the parton fractional momentum x_B , the four-momentum transfer squared and the atomic mass number A , as it was first observed by the European Muon Collaboration [5]. At the large hadron collider (LHC) energies, the most relevant effects are parton-density shadowing or gluon saturation, which can be described using modified parton distribution functions in the nucleus [6] or using the color glass condensate (CGC) effective theory [7, 8]. Partons can also lose energy in the early stages of the collision via initial-state radiation, thus modifying the centre-of-mass energy of the partonic system [9], or experience transverse momentum broadening due to multiple soft collisions before the $b\bar{b}$ pair is produced [10–12].

Measurements in proton–nucleus (p–A) collisions and their comparison to pp results provide a tool to constrain the CNM effects. To quantify these effects, the nuclear modification factor can be defined as the production cross section in p–A collisions (σ_{pA}) divided by that in pp collisions (σ_{pp}) scaled by the atomic mass number A

$$R_{pA}(y, p_T) = \frac{1}{A} \frac{d^2\sigma_{pA}/dydp_T}{d^2\sigma_{pp}/dydp_T}, \quad (1)$$

where y is the rapidity of the measured hadron in the nucleon–nucleon centre-of-mass frame, and p_T its transverse momentum. In the absence of nuclear effects R_{pA} is expected to equal unity.

Cross sections for beauty production in proton–nucleus collisions have been measured at fixed target experiments with beam energies of 800 and 920 GeV [13–15], corre-

* e-mail: alice-publications@cern.ch

sponding to nucleon-nucleon centre-of-mass energies up to $\sqrt{s_{\text{NN}}} = 41.6$ GeV. Measurements at the LHC in p–Pb collisions are sensitive to a previously unexplored parton kinematic domain of the colliding nucleons, in particular to small values of the gluonic content of the nucleon x_{B} . For instance, in the perturbative QCD leading order process $g g \rightarrow b\bar{b}$ the threshold production of a $b\bar{b}$ pair at $y = 0$ and $y = 3$ in p–Pb collisions at $\sqrt{s_{\text{NN}}} = 5.02$ TeV is obtained, respectively, for $x_{\text{B}} \approx 10^{-3}$ and 10^{-4} [16]. The LHCb experiment has measured beauty production at backward and forward rapidity [17, 18], where “forward” and “backward” are defined relative to the direction of the proton, reporting $R_{\text{pPb}} = 0.83 \pm 0.08$ at forward rapidity ($1.5 < y < 4$) and $R_{\text{pPb}} = 0.98 \pm 0.12$ at backward rapidity ($-5 < y < -2.5$) in p–Pb collisions at $\sqrt{s_{\text{NN}}} = 5.02$ TeV. Results at mid-rapidity have been reported from the ATLAS and CMS experiments, based on either exclusively reconstructed beauty mesons [19], or semi-inclusive decays $h_{\text{b}} \rightarrow J/\psi + X$ [20–22] or beauty jets [23]. These measurements however do not cover, at mid-rapidity, the low p_{T} region where the nuclear effects are expected to be the largest and the bulk of the total b-hadron production is concentrated. ALICE has measured beauty production in p–Pb collisions at $\sqrt{s_{\text{NN}}} = 5.02$ TeV through the semi-leptonic decay channel, $h_{\text{b}} \rightarrow e + X$, down to a transverse momentum of the decay electron of 1 GeV/c, finding R_{pPb} compatible with unity within large experimental uncertainties [24].

In this paper, the measurement of beauty production at mid-rapidity in p–Pb collisions at $\sqrt{s_{\text{NN}}} = 5.02$ TeV using the semi-inclusive channel $h_{\text{b}} \rightarrow J/\psi + X$ is presented. The J/ψ mesons are reconstructed in the dielectron decay channel, $J/\psi \rightarrow e^+e^-$, down to p_{T} of 1.3 GeV/c and for J/ψ rapidity in the nucleon-nucleon centre-of-mass system within $-1.37 < y < 0.43$. The covered p_{T} range corresponds to about 80% of the p_{T} -integrated cross section at mid-rapidity, $d\sigma/dy$, which allows to derive the p_{T} -integrated $b\bar{b}$ cross section $d\sigma_{b\bar{b}}/dy$ with extrapolation uncertainties of a few percent.

ALICE already reported measurements of inclusive J/ψ production at backward, mid- and forward rapidity in p–Pb collisions at $\sqrt{s_{\text{NN}}} = 5.02$ TeV down to $p_{\text{T}} = 0$ [25]. The production of the prompt J/ψ meson in hadronic interactions represents another test for QCD-inspired models (for comprehensive reviews see, e.g. [26, 27]). The inclusive J/ψ yield is composed of three contributions: prompt J/ψ produced directly in the p–Pb collision, prompt J/ψ produced indirectly (via the decay of heavier charmonium states such as χ_{c} and $\psi(2\text{S})$), and non-prompt J/ψ from the decay of long-lived b-hadrons. The precise vertexing capabilities of the ALICE detector allow us to determine the non-prompt component at mid-rapidity, which is discussed in this work. This measurement is combined with results on inclusive J/ψ production to determine the prompt J/ψ cross sections, which allow a more direct comparison with models describing the

charmonium production in hadronic interactions as compared to the inclusive J/ψ production.

2 Data sample and analysis

The ALICE apparatus [28, 29] consists of a central barrel, covering the pseudorapidity region $|\eta| < 0.9$, a muon spectrometer with $-4 < \eta < -2.5$ coverage, and forward and backward detectors employed for triggering, background rejection and event characterisation. The central-barrel detectors that have been used to reconstruct $J/\psi \rightarrow e^+e^-$ decays are the Inner Tracking System (ITS) and the Time Projection Chamber (TPC). They are located inside a large solenoidal magnet with a field strength of 0.5 T. The ITS [30] consists of six layers of silicon detectors surrounding the beam pipe at radial positions between 3.9 and 43.0 cm. Its two innermost layers are composed of Silicon Pixel Detectors (SPD), which provide the spatial resolution to separate on a statistical basis the prompt and non-prompt J/ψ components. The active volume of the TPC [31] covers the range along the beam direction $|z| < 250$ cm relative to the nominal interaction point and extends in radial direction from 85 cm to 247 cm. It is the main tracking device in the central barrel and, in addition, it is used for particle identification via the measurement of the specific energy loss (dE/dx) in the detector gas.

This analysis is based on the data sample collected during the 2013 LHC p–Pb run, corresponding to an integrated luminosity $\mathcal{L}_{\text{int}} = 51.4 \pm 1.9 \mu\text{b}^{-1}$. The events were selected using a minimum-bias trigger provided by the V0 detector [32], a system of two arrays of 32 scintillator tiles each covering the full azimuth within $2.8 < \eta < 5.1$ (V0A) and $-3.7 < \eta < -1.7$ (V0C). The trigger required at least one hit in both the V0A and the V0C scintillator arrays, and the non-single-diffractive p–Pb collisions were selected with an efficiency higher than 99%. A radiator-quartz detector, the T0 system [33], provided a measurement of the time of the collisions. The V0 and T0 time resolutions allowed discrimination of beam–beam interactions from background events in the interaction region. Further background suppression was applied in the offline analysis using temporal information from the neutron Zero Degree Calorimeters [34, 35].

The reconstruction of the J/ψ in the e^+e^- decay channel is described in detail in reference [25]. The tracks were reconstructed with the ITS and TPC detectors and required to have $p_{\text{T}} > 1.0$ GeV/c and $|\eta| < 0.9$, a minimum number of 70 TPC clusters per track (out of a maximum of 159), a χ^2 per space point of the track fit lower than 4, and at least one hit in the SPD. Electrons and positrons selection was based on the dE/dx values measured in the TPC: the dE/dx signal was required to be compatible with the mean electron energy loss within $\pm 3\sigma$, where σ denotes the resolution

of the dE/dx measurement. Furthermore, tracks consistent with the pion and proton assumptions were rejected. Electrons and positrons that, when paired, were found compatible with being result of photon conversions were also removed, in order to reduce the combinatorial background. It was verified, using a Monte Carlo simulation, that this procedure does not affect the J/ψ signal. J/ψ candidates were then obtained by pairing the selected positron and electron candidates in the same event and requiring the J/ψ rapidity to be within $-1.37 < y < 0.43$ (i.e. $|y_{\text{lab}}| < 0.9$ in the laboratory system). The condition that at least one of the two decay tracks has a hit in the innermost SPD layer was also required in order to enhance the resolution of the J/ψ decay vertices.

The measurement of the fraction of the J/ψ yield originating from b-hadron decays, f_b , relies on the discrimination of J/ψ mesons produced at a distance from the primary p-Pb collision vertex. The pseudoproper decay length variable x is defined as $x = c \cdot \vec{L} \cdot \vec{p}_T \cdot m_{J/\psi} / p_T$, where \vec{L} is the vector pointing from the primary vertex to the J/ψ decay vertex and $m_{J/\psi}$ is the J/ψ pole mass value [36]. The x resolution is about $150 \mu\text{m}$ ($60 \mu\text{m}$) for J/ψ of $p_T = 1.5 \text{ GeV}/c$ ($5 \text{ GeV}/c$). This allows to determine the fraction of J/ψ from the decay of b-hadrons for events with J/ψ p_T greater than $1.3 \text{ GeV}/c$. The same approach used in similar analyses for the pp [37] and Pb-Pb [38] colliding systems is adopted here. It is based on an unbinned two-dimensional fit, which is performed by minimising the opposite of the logarithm of the likelihood function $\mathcal{L}(m_{e^+e^-}, x)$,

$$-\ln \mathcal{L}(m_{e^+e^-}, x) = -\sum_1^N \ln \left[f_{\text{Sig}} \cdot F_{\text{Sig}}(x) \cdot M_{\text{Sig}}(m_{e^+e^-}) + (1 - f_{\text{Sig}}) \cdot F_{\text{Bkg}}(x) \cdot M_{\text{Bkg}}(m_{e^+e^-}) \right], \tag{2}$$

where N is the number of e^+e^- pairs in the invariant mass range $2.2 < m_{e^+e^-} < 4.0 \text{ GeV}/c^2$, $F_{\text{Sig}}(x)$ and $F_{\text{Bkg}}(x)$ are Probability Density Functions (PrDFs) describing the pseudoproper decay length distribution for signal (prompt and non-prompt J/ψ) and background candidates, respectively. Similarly, $M_{\text{Sig}}(m_{e^+e^-})$ and $M_{\text{Bkg}}(m_{e^+e^-})$ are the PrDFs describing the e^+e^- invariant mass distributions for the two components. The signal fraction f_{Sig} is defined as the ratio of the number of signal candidates over the sum of signal and background candidates. The fraction of non-prompt J/ψ enters into $F_{\text{Sig}}(x)$ as:

$$F_{\text{Sig}}(x) = f'_b \cdot F_b(x) + (1 - f'_b) \cdot F_{\text{prompt}}(x), \tag{3}$$

where $F_{\text{prompt}}(x)$ and $F_b(x)$ are the PrDFs for prompt and non-prompt J/ψ , respectively, and f'_b is the uncorrected fraction of J/ψ coming from b-hadron decays. A small correction due to the different acceptance times efficiency, averaged over p_T

in a given p_T interval ($\langle A \times \varepsilon \rangle$) for prompt and non-prompt J/ψ is necessary to obtain f_b from f'_b :

$$f_b = \left(1 + \frac{1 - f'_b}{f'_b} \frac{\langle A \times \varepsilon \rangle_b}{\langle A \times \varepsilon \rangle_{\text{prompt}}} \right)^{-1}. \tag{4}$$

The difference in $\langle A \times \varepsilon \rangle$ originates from the different p_T distributions of prompt and non-prompt J/ψ and the assumption on their spin alignment, as discussed later. The different components entering into the determination of f_b are described in detail in [37,38]. An improved procedure was introduced in this analysis to determine the resolution function, $R(x)$, which describes the accuracy by which x can be reconstructed and is the key ingredient of $F_{\text{prompt}}(x)$, $F_b(x)$ and $F_{\text{Bkg}}(x)$. $R(x)$ was determined using Monte Carlo simulations and considering the x distributions of prompt J/ψ reconstructed with the same procedure and selection criteria as for data. It was parameterised with a double-Gaussian core and a power function ($\propto |x|^{-\lambda}$) for the tails [37]. A tuning of the Monte Carlo simulation was applied to minimise the residual discrepancy between data and simulation for the distribution of the impact parameter of single charged tracks. The systematic uncertainty related to the incomplete knowledge of $R(x)$ was thus reduced, as discussed later.

In Fig. 1 the distributions of the invariant mass and the pseudoproper decay length for opposite-sign electron pairs with $p_T > 1.3 \text{ GeV}/c$ are shown with superimposed projections of the likelihood fit result. Although the J/ψ signal yield is not large, amounting to 360 counts for $p_T > 1.3 \text{ GeV}/c$, the data sample could be divided into three p_T intervals (1.3–3.0, 3.0–5.0 and 5.0–10 GeV/c), and the fraction f_b was evaluated in each interval with the same technique. At low p_T there are more candidates, but the resolution is worse and the signal over background, S/B , is smaller (i.e. f_{Sig} is smaller). At higher p_T the number of candidates is smaller, but the resolution improves and the background becomes minor. In Fig. 2 the distributions of the invariant mass and of the pseudoproper decay length are shown in different p_T intervals with superimposed projections of the best fit functions.

The values of the fraction of non-prompt J/ψ are evaluated with Eq. 4 assuming unpolarised prompt J/ψ . The relative variations of f_b expected in extreme scenarios for the polarisation of prompt J/ψ were studied in [37]. For non-prompt J/ψ , a small polarisation is obtained using EvtGen [39] as the result of the averaging effect caused by the admixture of various exclusive b-hadron decay channels. The extreme assumption of a null polarisation also for non-prompt J/ψ results in a relative decrease of f_b by only 1% at p_T of about 10 GeV/c and 4% at lower p_T (1.3–3.0 GeV/c). The uncertainties related to the polarisation of prompt and non-prompt J/ψ are not further propagated to the results, this choice being motivated by the small degree of polarisation measured in pp collisions at $\sqrt{s} = 7 \text{ TeV}$ [40–42].

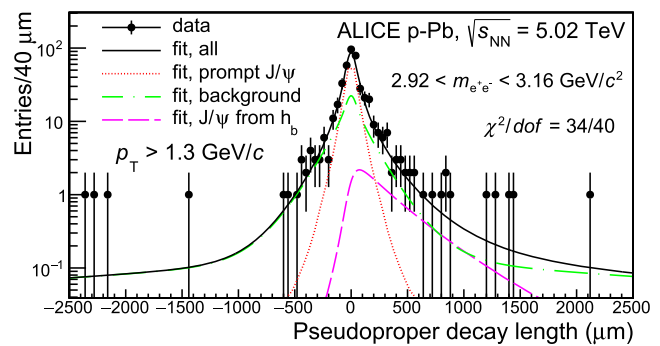
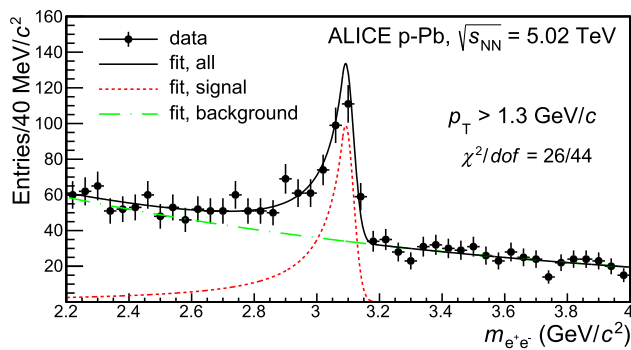


Fig. 1 Invariant mass (left panel) and pseudoproper decay length (right panel) distributions for J/ψ candidates with $p_T > 1.3$ GeV/ c with superimposed projections of the maximum likelihood fit. The latter dis-

tribution is limited to the J/ψ candidates under the mass peak, i.e. for $2.92 < m_{e^+e^-} < 3.16$ GeV/ c^2 , for display purposes only. The χ^2 values of these projections are also reported for both distributions

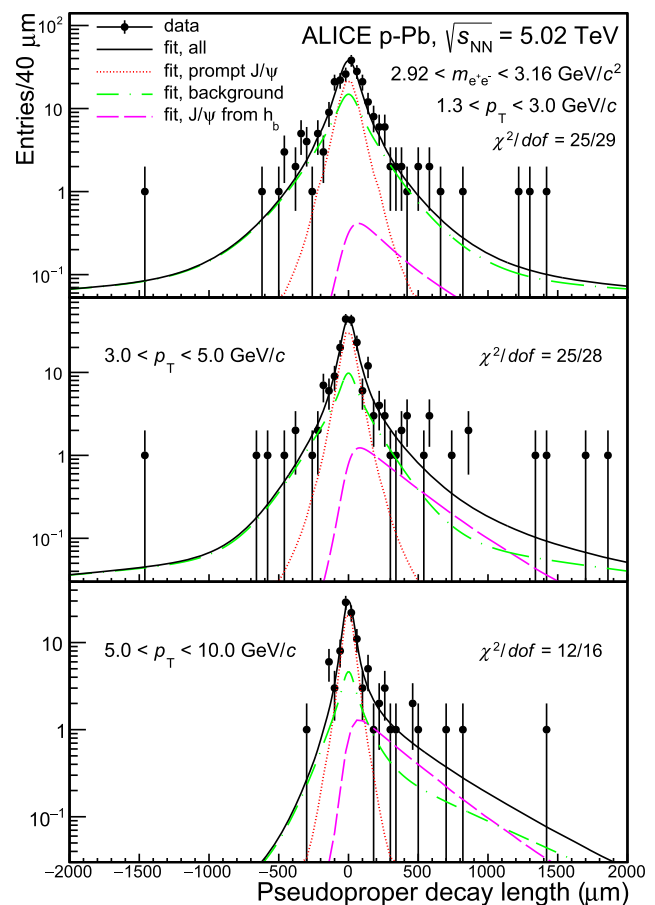
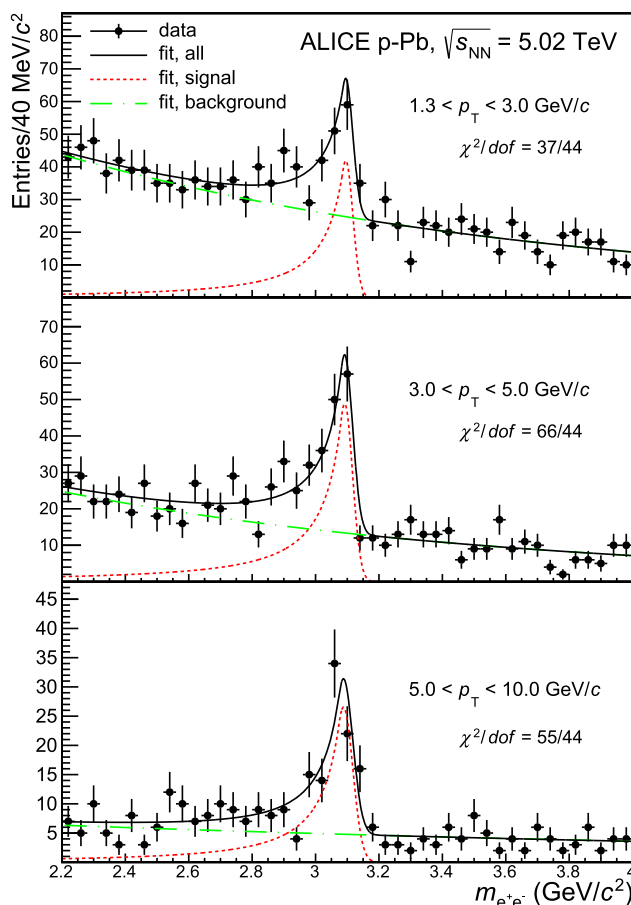


Fig. 2 Invariant mass (left panels) and pseudoproper decay length (right panels) distributions in different p_T intervals with superimposed projections of the maximum likelihood fit. The x distributions are lim-

ited to the J/ψ candidates under the mass peak. The χ^2 values of these projections are also reported for all distributions

The p_T and y distributions used as input to the Monte Carlo simulations assume for prompt J/ψ the shape from next-to-leading order (NLO) Color Evaporation Model (CEM) calculations [43–45], and take into account nuclear effects

according to the EPS09 parameterisation [46]. For the non-prompt J/ψ , b-hadrons were generated using PYTHIA 6.4.21 [47] with the Perugia-0 tune [48] and the nuclear shadowing provided by the EPS09 parameterisation was also

Table 1 Systematic uncertainties (in percent) on the measurement of the fraction f_b of J/ψ from the decay of b-hadrons, for different transverse momentum ranges. The symbol “–” is used to indicate a negligible contribution

Source	Systematic uncertainties (%)			
	p_T range (GeV/c)			
	> 1.3	1.3–3	3–5	5–10
Resolution function	6	20	4	3
PrDF for the x of non-prompt J/ψ	2	4	1	–
PrDF for the x of the background	7	16	6	6
MC p_T distributions	3	1	1	–
PrDF for the invariant mass of signal	6	7	4	3
PrDF for the invariant mass of background	3	8	2	1
Total	12	28	9	7

introduced. In both cases the signal events were injected into p–Pb collisions simulated with HIJING [49], and a full simulation of the detector response was performed adopting GEANT3 [50] as particle transport code. The particle decay was simulated with the EvtGen package [39], using the PHOTOS model [51] to properly describe the J/ψ radiative decay channel ($J/\psi \rightarrow e^+e^-\gamma$). The same reconstruction procedure and selection criteria were applied to simulated events as to real data.

The systematic uncertainties in the determination of f_b arise mainly from uncertainties on the resolution function, and the x and $m_{e^+e^-}$ PrDFs for background pairs, prompt and non-prompt J/ψ . They were estimated by propagating the residual discrepancy between Monte Carlo simulations and data, varying the functional forms assumed for the different PrDFs, and repeating the fitting procedure with similar approaches as those described in [37,38]. The uncertainty on the shape of the p_T distributions in the Monte Carlo simulations introduces also a systematic uncertainty in the determination of f_b . In fact, the Monte Carlo simulations have been used to determine p_T -dependent quantities that were averaged over finite-size p_T intervals as, e.g. $\langle A \times \varepsilon \rangle$, and the result of the average depends on the p_T shape. Different assumptions for the p_T distributions were considered, resulting in variations for the average p_T of $\sim 15\%$ for both prompt and non-prompt components in the p_T integrated sample. These include cases without nuclear shadowing, a parameterisation of the non-prompt component from perturbative QCD calculations at fixed order with next-to-leading-log re-summation (FONLL) [52] and a parameterisation of the prompt component with the phenomenological function defined in [53]. Due to the weak p_T dependence of $A \times \varepsilon$, this uncertainty is found to be significant only for the p_T -integrated case.¹ Table 1 summarises the systematic uncer-

tainties for the p_T -integrated result ($p_T > 1.3$ GeV/c) and the three p_T intervals.

The value of f_b in pp collisions at $\sqrt{s} = 5.02$ TeV, f_b^{pp} , is needed to compute the R_{pPb} for prompt and non-prompt J/ψ mesons,

$$R_{\text{pPb}} = \frac{1 - f_b^{\text{pPb}}}{1 - f_b^{\text{pp}}} R_{\text{pPb}}^{\text{incl. } J/\psi} \quad \text{for prompt } J/\psi \quad \text{and} \quad (5)$$

$$R_{\text{pPb}} = \frac{f_b^{\text{pPb}}}{f_b^{\text{pp}}} R_{\text{pPb}}^{\text{incl. } J/\psi} \quad \text{for non-prompt } J/\psi,$$

where $R_{\text{pPb}}^{\text{incl. } J/\psi}$ is the nuclear modification factor for inclusive J/ψ measured in [25]. The same interpolation procedure implemented to derive f_b^{pp} at $\sqrt{s} = 2.76$ TeV [38] was used to determine f_b^{pp} at $\sqrt{s} = 5.02$ TeV. It is based on experimental data (mostly shown in Fig. 3) from CDF in $p\bar{p}$ collisions [57] at lower centre-of-mass energy (1.96 TeV) and from ALICE [37], ATLAS [58] and CMS [59] in pp collisions at higher energy (7 TeV). The value for $p_T > 1.3$ GeV/c is $f_b^{\text{pp}} = 0.139 \pm 0.013$. The values obtained in other p_T intervals are reported in the central column of Table 2.

3 Results

The fraction of J/ψ yield originating from decays of b-hadrons in the experimentally accessible kinematic range, $p_t > 1.3$ GeV/c and $-1.37 < y < 0.43$, which is referred to as “visible region” in the following, is found to be

$$f_b = 0.105 \pm 0.038 (\text{stat.}) \pm 0.012 (\text{syst.}).$$

Footnote 1 continued

recently delivered by the same authors [54]. Another set of nuclear PDF, nCTEQ15, was also released [55] and adopted in recent model computations [56]. The EPS09 parameterisation was used in the Monte Carlo simulation to derive the central value of $A \times \varepsilon$, but the alternative assumptions that have been considered produce larger deviations in the p_T distributions than those obtained using either EPPS16 or nCTEQ15 instead of EPS09.

¹ A new parameterisation of the nuclear modifications to the PDF, which supersedes EPS09 and has been named as EPPS16, has been

Table 2 Fraction of non-prompt J/ψ in pp collisions at $\sqrt{s} = 5.02$ TeV for different p_T ranges, as determined with the procedure of interpolation described in [38], and that measured in p–Pb collisions in this analysis. For the latter, the first uncertainty is statistical, the second one is systematical. The upper limit at 95% confidence level is given for the interval $1.3 < p_T < 3$ GeV/c

p_T range (GeV/c)	f_b^{pp} at $\sqrt{s} = 5.02$ TeV	f_b^{pPb} at $\sqrt{s_{NN}} = 5.02$ TeV
> 0	0.134 ± 0.013	–
> 1.3	0.139 ± 0.013	$0.105 \pm 0.038 \pm 0.012$
$1.3\text{--}3$	0.118 ± 0.013	< 0.175 at 95% C.L.
$3\text{--}5$	0.143 ± 0.012	$0.123 \pm 0.052 \pm 0.011$
$5\text{--}10$	0.202 ± 0.013	$0.203 \pm 0.070 \pm 0.014$

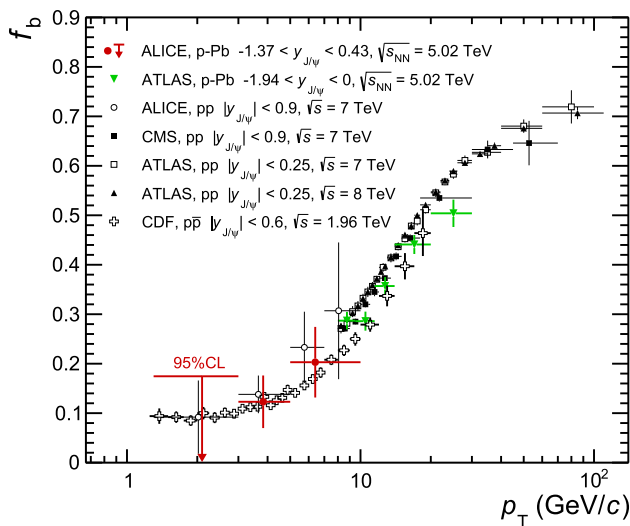


Fig. 3 Fraction of J/ψ from the decay of b-hadrons at mid-rapidity as a function of the p_T of J/ψ in p–Pb collisions at $\sqrt{s_{NN}} = 5.02$ TeV compared with results from ATLAS [20] in the same colliding system and results of ALICE [37], ATLAS [60] and CMS [59] in pp collisions at either $\sqrt{s} = 7$ TeV or $\sqrt{s} = 8$ TeV. Results from CDF [57] in $p\bar{p}$ collisions at $\sqrt{s} = 1.96$ TeV are also shown. The ALICE data symbols are placed horizontally at the average value of the p_T distribution of each interval (see text for details). For all experiments, the vertical error bars represent the quadratic sum of the statistical and systematic errors. In the interval $1.3 < p_T < 3$ GeV/c the upper limit at the 95% confidence level is shown, as discussed in the text

The results in the different p_T intervals are reported in Table 2. In the interval $1.3 < p_T < 3$ GeV/c the minimum of Eq. 2, which is obtained for $f_b = 0.05$, is broad and it was not possible to define 1σ symmetric uncertainty bounds within the physical region $f_b > 0$. Therefore an upper limit at the 95% confidence level was derived assuming normally distributed uncertainties. Figure 3 shows the fraction of non-prompt J/ψ as a function of p_T compared to the results of ATLAS [20] covering the high p_T region ($p_T > 8$ GeV/c) in a similar rapidity range ($-1.94 < y < 0$). In the figure, the ALICE data symbols are placed horizontally at the average value of the p_T distribution of each interval. The

average was computed using the Monte Carlo simulations, which are described in the previous section, weighted by the measured f_b . In Fig. 3 the results of CDF [57] for $p\bar{p}$ collisions at $\sqrt{s} = 1.96$ TeV and of ALICE [37], ATLAS [60] and CMS [59] experiments in pp collisions at either $\sqrt{s} = 7$ or $\sqrt{s} = 8$ TeV are also shown.

By combining the measurement of inclusive J/ψ cross sections [25] with the f_b determinations, the prompt and non-prompt J/ψ production cross sections were obtained as follows:

$$\sigma_{J/\psi \text{ from } h_b} = f_b \cdot \sigma_{J/\psi}, \quad \sigma_{\text{prompt } J/\psi} = (1 - f_b) \cdot \sigma_{J/\psi}. \tag{6}$$

In the visible region the following value is derived for the non-prompt component:

$$\sigma_{J/\psi \text{ from } h_b}^{\text{vis}} = 138 \pm 51(\text{stat.}) \pm 19(\text{syst.}) \mu\text{b}.$$

The visible cross section of non-prompt J/ψ production was extrapolated down to $p_T = 0$ using FONLL calculations [52] with CTEQ6.6 PDFs [61] and nuclear modification of the parton distribution functions (nPDFs) from the EPPS16 parameterisation [54]. The fragmentation of b-quarks into hadrons was performed using PYTHIA 6.4.21 [47] with the Perugia-0 tune [48]. The extrapolation factor, which is equal to $1.22_{-0.04}^{+0.02}$, was computed as the ratio of the cross section for $p_T^{J/\psi} > 0$ and $-1.37 < y < 0.43$ to that in the visible region. The uncertainty on the extrapolation factor was determined by combining the FONLL, CTEQ6.6 and EPPS16 uncertainties. The FONLL uncertainties have been evaluated by varying the factorisation and renormalisation scales, μ_F and μ_R , independently in the ranges $0.5 < \mu_F/m_T < 2$, $0.5 < \mu_R/m_T < 2$, with the constraint $0.5 < \mu_F/\mu_R < 2$, where $m_T = \sqrt{p_T^2 + m_b^2}$. The b-quark mass was varied within $4.5 < m_b < 5.0$ GeV/c². The CTEQ6.6 and EPPS16 uncertainties were propagated according to the Hessians prescription of the authors of these parameterisations (Eq. 53 of reference [54]). The extrapolated p_T -integrated non-prompt J/ψ cross section per unit of rapidity is obtained by dividing by the rapidity range $\Delta y = 1.8$:

$$\frac{d\sigma_{J/\psi \text{ from } h_b}}{dy} = 93 \pm 35(\text{stat.}) \pm 13(\text{syst.})_{-3}^{+2}(\text{extr.}) \mu\text{b}.$$

In the left panel of Fig. 4 this measurement is plotted together with the LHCb [17] results and compared to theoretical predictions based on FONLL pQCD calculations with EPPS16 nPDFs. The empty band shows the total theoretical uncertainties, while the coloured band corresponds to the contribution from the EPPS16 uncertainties. The cross section was also computed, according to Eq. 6, in the three p_T intervals and compared to the ATLAS measurements [20] for $-1.94 < y < 0$ and $p_T > 8$ GeV/c (right panel of Fig. 4). The ALICE measurement, which covers the low p_T region at

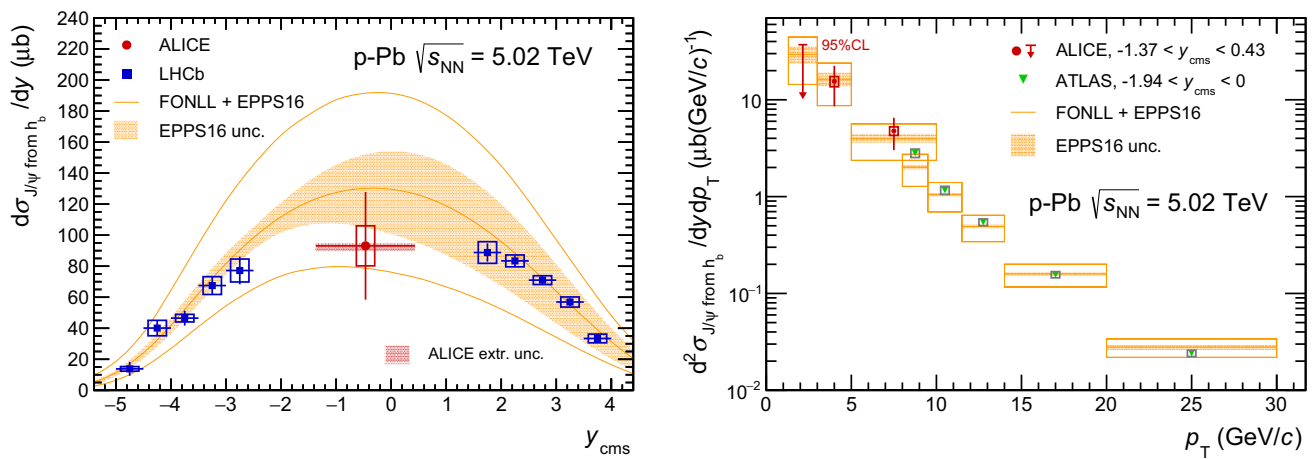


Fig. 4 $d\sigma_{J/\psi \text{ from } h_b}/dy$ as a function of y (left panel) compared to results obtained in the forward and backward rapidity regions by LHCb [17] and $d^2\sigma_{J/\psi \text{ from } h_b}/dy dp_T$ as a function of p_T (right panel) compared to ATLAS results [20]. The error bars represent the statistical uncertainties, while the systematic uncertainties are shown as boxes. In the right panel, the upper limit at the 95% confidence level is shown

mid-rapidity, is thus complementary to the data of the other LHC experiments. The total theoretical uncertainties on the production cross section, which are dominated by those of the b-quark mass and the QCD factorisation and renormalisation scales, are larger than the experimental uncertainties, preventing to draw conclusions on the presence of nuclear effects for this observable.

The dominant uncertainties of the theoretical predictions cancel out when considering the nuclear modification factor R_{pPb} , which was determined experimentally according to Eq. 5. Figure 5 shows the R_{pPb} of non-prompt J/ψ for $p_T > 0$ as compared to the LHCb measurements at backward and forward rapidity [17] (left panel) and as a function of p_T as compared to CMS results [21] (right panel). The results are also compared to the FONLL pQCD calculations with EPPS16 nPDFs described previously. The central value of an alternative parameterisation of the nuclear PDF, nDSgLO [62], is also shown for comparison in the left-hand plot. The p_T -integrated R_{pPb} , which is $R_{pPb} = 0.54 \pm 0.20(\text{stat.}) \pm 0.13(\text{syst.})_{-0.02}^{+0.01}(\text{extr.})$, is measured to be smaller than unity with a significance of 2.3/3.5/1.9 σ (statistical/systematic/combined). The p_T dependence suggests that the suppression of the production originates at low p_T .

The $b\bar{b}$ production cross section at mid-rapidity was obtained as

$$\frac{d\sigma_{b\bar{b}}}{dy} = \frac{d\sigma_{b\bar{b}}^{\text{model}}}{dy} \times \frac{\sigma_{J/\psi \text{ from } h_b}^{\text{vis}}}{\sigma_{J/\psi \text{ from } h_b}^{\text{vis, model}}}, \tag{7}$$

where $d\sigma_{b\bar{b}}^{\text{model}}/dy$ and $\sigma_{J/\psi \text{ from } h_b}^{\text{vis, model}}$ were again obtained performing FONLL plus CTEQ6.6 and EPPS16 calculations.

with an arrow for the interval $1.3 < p_T < 3 \text{ GeV}/c$. The systematic uncertainty on the extrapolation to $p_T = 0$ (left panel only) is indicated by the filled red box. Results from FONLL computations [52] with EPPS16 [54] nuclear modification of the CTEQ6.6 PDFs [61] are shown superimposed, including the total theoretical uncertainty (empty band/boxes) and the EPPS16 contribution (coloured band/boxes)

The average branching fraction of inclusive b-hadron decays to J/ψ measured at LEP [63–65], $BR(h_b \rightarrow J/\psi + X) = (1.16 \pm 0.10)\%$, was used in the computation of $\sigma_{J/\psi \text{ from } h_b}^{\text{model}}$. The resulting cross section at mid-rapidity is

$$\frac{d\sigma_{b\bar{b}}}{dy} = 4.1 \pm 1.5(\text{stat.}) \pm 0.7(\text{syst.})_{-0.2}^{+0.1}(\text{extr.}) \text{ mb.}$$

The total $b\bar{b}$ production cross section was computed similarly by extrapolating the visible cross section to the full phase space as

$$\sigma(pPb \rightarrow b\bar{b} + X) = \alpha_{4\pi} \frac{\sigma_{J/\psi \text{ from } h_b}^{\text{vis}}}{2 \cdot BR(h_b \rightarrow J/\psi + X)}, \tag{8}$$

where $\alpha_{4\pi}$ is the ratio between the yield of J/ψ mesons (from the decay of b-hadrons) in the full phase space and the yield in the visible region, and the factor 2 takes into account that b-hadrons originate from both b and \bar{b} quarks. The extrapolation factor $\alpha_{4\pi}$ was also computed based on FONLL pQCD calculations with EPPS16 nPDFs, with the b-quark fragmentation performed using PYTHIA 6.4.21 with the Perugia-0 tune, and found to be $\alpha_{4\pi} = 4.1 \pm 0.2$. The resulting cross section is

$$\sigma(pPb \rightarrow b\bar{b} + X) = 25 \pm 9(\text{stat.}) \pm 4(\text{syst.}) \pm 1(\text{extr.}) \text{ mb (ALICE only).}$$

The ALICE measurement is shown in Fig. 6 along with the other existing measurements in p-A collisions, which were obtained in fixed-target experiments [13–15] at lower $\sqrt{s_{NN}}$. The experimental results are compared to the FONLL calculations using the EPPS16 nPDFs.

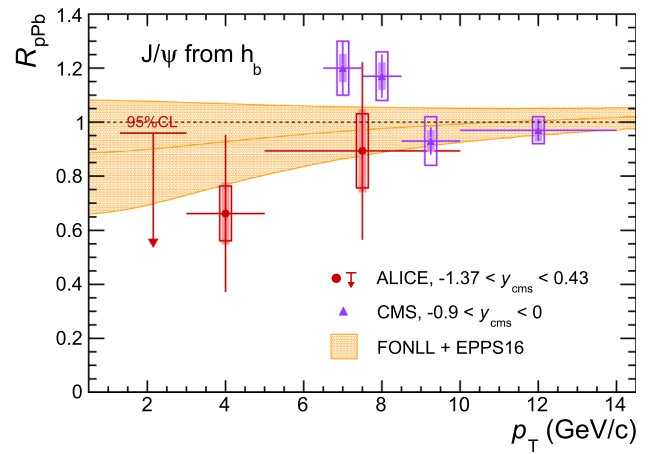
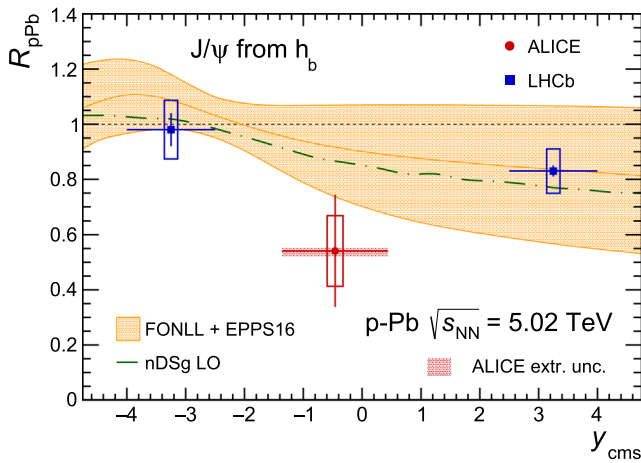


Fig. 5 The nuclear modification factor R_{pPb} of non-prompt J/ψ as a function of rapidity for $p_T > 0$ (left panel) and as a function of p_T at mid-rapidity (right panel). The error bars and the open boxes indicate, respectively, the statistical and systematic uncertainties. In the left hand panel, the results from the LHCb experiment are taken from [17] and the systematic uncertainty on the extrapolation to $p_T = 0$ for the

ALICE data point is depicted by the filled red box. In the right hand plot, the results from the CMS experiment are taken from [21] and the arrow shows the upper limit at 95% confidence level for the interval $1.3 < p_T < 3$ GeV/c. The nuclear modification factors as expected from the EPPS16 [54] and the nDSg [62] (central value shown in the left panel only) parameterisations are shown superimposed

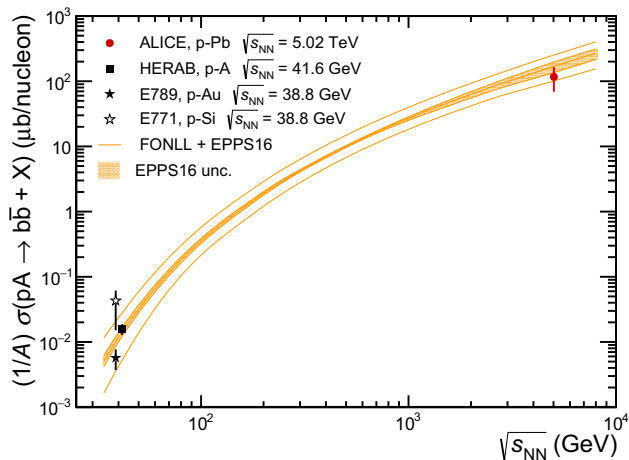


Fig. 6 Beauty production cross section in p-A collisions as a function of $\sqrt{s_{NN}}$ as measured by ALICE and at fixed-target experiments (E789 [13], E771 [14] and HERA-B [15]). The FONLL calculations with EPPS16 nuclear modification to the PDFs are superimposed in orange. The full lines show the total theoretical uncertainty, while the coloured band corresponds to the contribution from the EPPS16 uncertainties

The combination with the LHCb measurements [17] allows us to extract the total $b\bar{b}$ cross section with a significant reduction of the uncertainty. The factor $\alpha_{4\pi}$, which is computed as the ratio of the yield in full phase space over that covered by ALICE and LHCb, reduces to $1.60^{+0.02}_{-0.03}$ and the total cross section becomes

$$\sigma(pPb \rightarrow b\bar{b} + X) = 29 \pm 4(\text{stat.}) \pm 3(\text{syst.}) \pm 1(\text{extr.}) \text{ mb (ALICE and LHCb)}$$

Table 3 The production cross section of prompt J/ψ as a function of p_T in p-Pb collisions at $\sqrt{s_{NN}} = 5.02$ TeV measured for $-1.37 < y < 0.43$. The first quoted uncertainty is statistical, the second (third) is the systematical one that is correlated (uncorrelated) in p_T

p_T (GeV/c)	$d^2\sigma^{\text{prompt } J/\psi} / dy dp_T$ ($\mu\text{b}/(\text{GeV}/c)$)
1.3 – 3.0	$200 \pm 35 \pm 25 \pm 8$
3.0 – 5.0	$111 \pm 15 \pm 8 \pm 4$
5.0 – 10.0	$18.7 \pm 2.9 \pm 1.2 \pm 0.7$

The production cross section of prompt J/ψ , $d\sigma_{\text{prompt } J/\psi} / dy$, was obtained by subtracting the cross section of J/ψ coming from b-hadron decays from the inclusive J/ψ one measured for $p_T > 0$ [25]:

$$\frac{d\sigma_{\text{prompt } J/\psi}}{dy} = 816 \pm 78(\text{stat.}) \pm 65(\text{syst.})^{+2}_{-3}(\text{extr.}) \mu\text{b}$$

The p_T differential cross section was derived using Eq. 6. The numerical values are reported in Table 3.

The nuclear modification factor for prompt J/ψ was computed using Eq. 5. With respect to the results discussed in [25], where the inclusive J/ψ production in p-Pb collisions at $\sqrt{s_{NN}} = 5.02$ TeV was presented, a more direct comparison with model predictions can now be performed. Figure 7 shows the R_{pPb} of prompt J/ψ compared to predictions from various models. The results indicate that the suppression observed at mid-rapidity is a low p_T effect, as also argued for non-prompt J/ψ . One calculation (Vogt [45,66]) is based on the NLO CEM for the prompt J/ψ production and the EPS09 NLO shadowing parameterisation. The the-

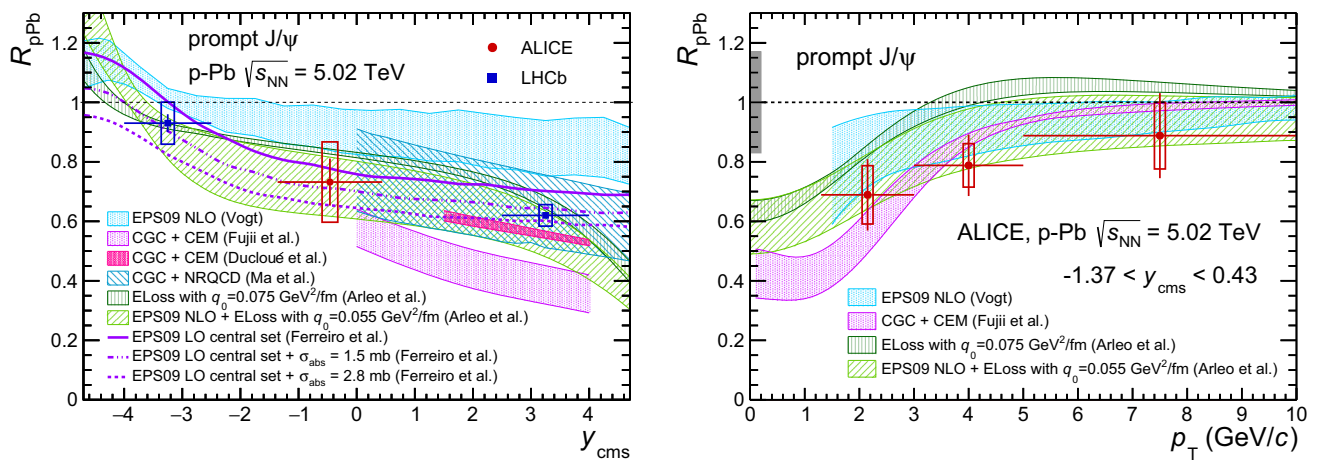


Fig. 7 R_{pPb} of prompt J/ψ versus rapidity (left panel) and as a function of p_T at mid-rapidity (right panel), compared to theoretical calculations. Statistical uncertainties are represented by vertical error bars, while open boxes correspond to systematic uncertainties. Results from

oretical uncertainties arise from those in EPS09 and from the values of the charm quark mass and of the renormalisation and factorisation scales. A second calculation (Arleo et al. [67]) is based on a parameterisation of experimental results on prompt J/ψ production in pp collisions, including the effects of coherent energy loss in the cold nuclear medium with or without introducing shadowing effects according to the EPS09 NLO parameterisation. The model of Ferreiro et al. [68] employs the EPS09 leading order (LO) nPDF with or without effects from the interaction with a nuclear medium. The last set of models are based on different implementations of the CGC effective theory, which assumes a regime of gluon saturation (see [7,8] for reviews), by using either the CEM for the prompt J/ψ production (Fujii et al. [69] and Ducloué et al. [70]) or the non-relativistic QCD (NRQCD) factorisation approach [71] (Ma et al. [72]). The results suggest the presence of nuclear effects in the low p_T region, but the present uncertainties do not allow us to discriminate among the different models.

4 Summary

The production of b-hadrons in p–Pb collisions at $\sqrt{s_{NN}} = 5.02$ TeV through the inclusive decay channel $h_b \rightarrow J/\psi + X$ has been measured at mid-rapidity and down to J/ψ p_T of 1.3 GeV/c. The mid-rapidity $d\sigma_{b\bar{b}}/dy$ and the total $b\bar{b}$ cross section, $\sigma_{b\bar{b}}$, were derived. The nuclear modification factor of beauty production at mid-rapidity, integrated over p_T , is $R_{pPb} = 0.54 \pm 0.20(\text{stat.}) \pm 0.13(\text{syst.})_{-0.02}^{+0.01}(\text{extr.})$ and compatible within uncertainties to expectations from the EPPS16 parameterisation of the nuclear modification to the PDFs. The production cross section of prompt J/ψ was obtained by subtracting the non-prompt component from

the LHCb experiment at backward and forward rapidity are shown in the left panel [17]. The box around $R_{pPb} = 1$ in the right panel shows the size of the correlated relative uncertainty. Results from various models [45,66–70,72,73] are also shown, see text for details

a previous measurement of the inclusive J/ψ production. The nuclear modification factor of prompt J/ψ indicates a reduced production of low p_T J/ψ , with respect to expectations from scaled pp collisions, but the present uncertainties do not allow us to discriminate among different models.

Acknowledgements The ALICE Collaboration would like to thank all its engineers and technicians for their invaluable contributions to the construction of the experiment and the CERN accelerator teams for the outstanding performance of the LHC complex. The ALICE Collaboration gratefully acknowledges the resources and support provided by all Grid centres and the Worldwide LHC Computing Grid (WLCG) collaboration. The ALICE Collaboration acknowledges the following funding agencies for their support in building and running the ALICE detector: A. I. Alikhanyan National Science Laboratory (Yerevan Physics Institute) Foundation (ANSI), State Committee of Science and World Federation of Scientists (WFS), Armenia; Austrian Academy of Sciences and Nationalstiftung für Forschung, Technologie und Entwicklung, Austria; Ministry of Communications and High Technologies, National Nuclear Research Center, Azerbaijan; Conselho Nacional de Desenvolvimento Científico e Tecnológico (CNPq), Universidade Federal do Rio Grande do Sul (UFRGS), Financiadora de Estudos e Projetos (Finep) and Fundação de Amparo à Pesquisa do Estado de São Paulo (FAPESP), Brazil; Ministry of Science & Technology of China (MSTC), National Natural Science Foundation of China (NSFC) and Ministry of Education of China (MOEC), China; Ministry of Science, Education and Sport and Croatian Science Foundation, Croatia; Ministry of Education, Youth and Sports of the Czech Republic, Czech Republic; The Danish Council for Independent Research | Natural Sciences, the Carlsberg Foundation and Danish National Research Foundation (DNRF), Denmark; Helsinki Institute of Physics (HIP), Finland; Commissariat à l’Énergie Atomique (CEA) and Institut National de Physique Nucléaire et de Physique des Particules (IN2P3) and Centre National de la Recherche Scientifique (CNRS), France; Bundesministerium für Bildung, Wissenschaft, Forschung und Technologie (BMBF) and GSI Helmholtzzentrum für Schwerionenforschung GmbH, Germany; General Secretariat for Research and Technology, Ministry of Education, Research and Religions, Greece; National Research, Development and Innovation Office, Hungary; Department of Atomic Energy

Government of India (DAE), Department of Science and Technology, Government of India (DST), University Grants Commission, Government of India (UGC) and Council of Scientific and Industrial Research (CSIR), India; Indonesian Institute of Science, Indonesia; Centro Fermi - Museo Storico della Fisica e Centro Studi e Ricerche Enrico Fermi and Istituto Nazionale di Fisica Nucleare (INFN), Italy; Institute for Innovative Science and Technology, Nagasaki Institute of Applied Science (IIST), Japan Society for the Promotion of Science (JSPS) KAKENHI and Japanese Ministry of Education, Culture, Sports, Science and Technology (MEXT), Japan; Consejo Nacional de Ciencia (CONACYT) y Tecnología, through Fondo de Cooperación Internacional en Ciencia y Tecnología (FONCICYT) and Dirección General de Asuntos del Personal Académico (DGAPA), Mexico; Nederlandse Organisatie voor Wetenschappelijk Onderzoek (NWO), Netherlands; The Research Council of Norway, Norway; Commission on Science and Technology for Sustainable Development in the South (COMSATS), Pakistan; Pontificia Universidad Católica del Perú, Peru; Ministry of Science and Higher Education and National Science Centre, Poland; Korea Institute of Science and Technology Information and National Research Foundation of Korea (NRF), Republic of Korea; Ministry of Education and Scientific Research, Institute of Atomic Physics and Romanian National Agency for Science, Technology and Innovation, Romania; Joint Institute for Nuclear Research (JINR), Ministry of Education and Science of the Russian Federation and National Research Centre Kurchatov Institute, Russia; Ministry of Education, Science, Research and Sport of the Slovak Republic, Slovakia; National Research Foundation of South Africa, South Africa; Centro de Aplicaciones Tecnológicas y Desarrollo Nuclear (CEADEN), Cubaenergía, Cuba and Centro de Investigaciones Energéticas, Medioambientales y Tecnológicas (CIEMAT), Spain; Swedish Research Council (VR) and Knut & Alice Wallenberg Foundation (KAW), Sweden; European Organization for Nuclear Research, Switzerland; National Science and Technology Development Agency (NSDTA), Suranaree University of Technology (SUT) and Office of the Higher Education Commission under NRU project of Thailand, Thailand; Turkish Atomic Energy Agency (TAEK), Turkey; National Academy of Sciences of Ukraine, Ukraine; Science and Technology Facilities Council (STFC), United Kingdom; National Science Foundation of the United States of America (NSF) and United States Department of Energy, Office of Nuclear Physics (DOE NP), United States of America.

Open Access This article is distributed under the terms of the Creative Commons Attribution 4.0 International License (<http://creativecommons.org/licenses/by/4.0/>), which permits unrestricted use, distribution, and reproduction in any medium, provided you give appropriate credit to the original author(s) and the source, provide a link to the Creative Commons license, and indicate if changes were made. Funded by SCOAP³.

References

- J.C. Collins, D.E. Soper, G.F. Sterman, Factorization of hard processes in QCD. *Adv. Ser. Direct. High Energy Phys.* **5**, 1–91 (1989). [arXiv:hep-ph/0409313](#)
- S. Catani, M. Ciafaloni, F. Hautmann, High-energy factorization and small x heavy flavor production. *Nucl. Phys. B* **336**, 135–188 (1991)
- N. Cabibbo, G. Parisi, Exponential hadronic spectrum and quark liberation. *Phys. Lett. B* **59**, 67 (1975)
- E.V. Shuryak, Quark–gluon plasma and hadronic production of leptons, photons and pions. *Phys. Lett. B* **150**, 150 (1978)
- European Muon Collaboration, The ratio of the nucleon structure functions f_2^n for iron and deuterium. *Phys. Lett. B* **123**, 275 (1983)
- N. Armesto, Nuclear shadowing. *J. Phys. G* **32**, R367 (2016). [arXiv:hep-ph/0604108](#)
- J.-P. Blaizot, F. Gelis, R. Venugopalan, High energy pA collisions in the color glass condensate approach II: quark pair production. *Nucl. Phys. A* **743**, 57 (2004). [arXiv:hep-ph/0402257](#)
- F. Gelis, Color glass condensate and glasma. *Int. J. Mod. Phys. A* **28**, 1330001 (2013). [arXiv:1211.3327 \[hep-ph\]](#)
- I. Vitev, Non-Abelian energy loss in cold nuclear matter. *Phys. Rev. C* **75**, 064906 (2007). [arXiv:hep-th/0703002](#)
- M. Lev, B. Petersson, Nuclear effects at large transverse momentum in a QCD parton model. *Z. Phys. C* **21**, 155 (1983)
- X. Wang, Systematic study of high p_T hadron spectra in pp, pA, and AA collisions at ultrarelativistic energies. *Phys. Rev. C* **61**, 064910 (2000). [arXiv:nucl-th/9812021](#)
- B. Kopeliovich, J. Nemchik, A. Schäfer, A. Tarasov, Cronin effect in hadron production off nuclei. *Phys. Rev. Lett.* **88**, 232303 (2002). [arXiv:hep-ph/0201010](#)
- E789 Collaboration, Measurement of the bottom-quark production cross section in 800 GeV/c proton–gold collisions. *Phys. Rev. Lett.* **74**, 3118 (1995)
- E771 Collaboration, Measurement of the $b\bar{b}$ cross section in 800 GeV/c proton–silicon interactions. *Phys. Rev. Lett.* **82**, 41 (1999)
- HERA-B Collaboration, Bottom production cross section from double muonic decays of b-flavoured hadrons in 920 GeV proton–nucleus collisions. *Phys. Lett. B.* **650**, 103 (2007). [arXiv:hep-ex/0612024](#)
- ALICE Collaboration, ALICE: physics performance report, volume II. *J. Phys. G* **32**, 1295 (2006)
- LHCb Collaboration, Study of J/ψ production and cold nuclear matter effects in pPb collisions at $\sqrt{s_{NN}} = 5$ TeV. *J. High Energy Phys.* **02**, 072 (2014). [arXiv:1308.6729 \[nucl-ex\]](#)
- LHCb Collaboration, Prompt and nonprompt J/ψ production and nuclear modification in pPb collisions at $\sqrt{s_{NN}} = 8.16$ TeV. *Phys. Lett. B* **774**, 159 (2017). [arXiv:1706.07122 \[hep-ex\]](#)
- CMS Collaboration, Study of B meson production in p + Pb collisions at $\sqrt{s_{NN}} = 5.02$ TeV using exclusive hadronic decays. *Phys. Rev. Lett.* **116**, 032301 (2016). [arXiv:1508.06678 \[nucl-ex\]](#)
- ATLAS Collaboration, Measurement of differential J/ψ production cross sections and forward–backward ratios in p + Pb collisions with the ATLAS detector. *Phys. Rev. C* **92**, 034904 (2015). [arXiv:1505.08141 \[hep-ex\]](#)
- CMS Collaboration, Measurement of prompt and non-prompt J/ψ production in pp and pPb collisions at $\sqrt{s_{NN}} = 5.02$ TeV. *Eur. Phys. J. C* **77**, 269 (2017). [arXiv:1702.01462 \[nucl-ex\]](#)
- ATLAS Collaboration, Measurement of quarkonium production in proton–lead and proton–proton collisions at 5.02 TeV with the ATLAS detector. [arXiv:1709.03089 \[nucl-ex\]](#)
- CMS Collaboration, Transverse momentum spectra of inclusive b jets in p–Pb collisions at $\sqrt{s_{NN}} = 5.02$ TeV. *Phys. Lett. B* **754**, 59 (2016). [arXiv:1510.03373 \[nucl-ex\]](#)
- ALICE Collaboration, Measurement of electrons from beauty-hadron decays in p–Pb collisions at $\sqrt{s_{NN}} = 5.02$ TeV and Pb–Pb collisions at $\sqrt{s_{NN}} = 2.76$ TeV. *J. High Energy Phys.* **07**, 52 (2017). [arXiv:1609.03898 \[nucl-ex\]](#)
- ALICE Collaboration, Rapidity and transverse-momentum dependence of the inclusive J/ψ nuclear modification factor in p–Pb collisions at $\sqrt{s_{NN}} = 5.02$ TeV. *J. High Energy Phys.* **06**, 055 (2015). [arXiv:1503.07179 \[nucl-ex\]](#)
- N. Brambilla et al., Heavy quarkonium: progress, puzzles, and opportunities. *Eur. Phys. J. C* **71**, 1534 (2011). [arXiv:1010.5827 \[hep-ph\]](#)

27. A. Andronic et al., Heavy-flavour and quarkonium production in the LHC era: from proton–proton to heavy-ion collisions. *Eur. Phys. J. C* **76**, 107 (2016). [arXiv:1506.03981](#) [nucl-ex]
28. ALICE Collaboration, The ALICE experiment at the CERN LHC. *J. Instrum.* **3**(08), S08002 (2008)
29. ALICE Collaboration, Performance of the ALICE experiment at the CERN LHC. *Int. J. Mod. Phys. A* **29**, 1430044 (2014). [arXiv:1402.4476](#) [nucl-ex]
30. ALICE Collaboration, Alignment of the ALICE inner tracking system with cosmic-ray tracks. *JINST* **5**, P03003 (2010). [arXiv:1001.0502](#) [physics.ins-det]
31. J. Alme et al., The ALICE TPC, a large 3-dimensional tracking device with fast readout for ultra-high multiplicity events. *Nucl. Instrum. Methods A* **622**, 316 (2010)
32. ALICE Collaboration, Performance of the ALICE VZERO system. *JINST* **8**, P10016 (2013). [arXiv:1306.3130](#) [nucl-ex]
33. ALICE Collaboration, ALICE forward detectors: FMD, T0 and V0. Technical Design Report, CERN-LHCC-2004-025. <https://cds.cern.ch/record/781854>
34. ALICE Collaboration, Measurement of the cross section for electromagnetic dissociation with neutron emission in Pb–Pb collisions at $\sqrt{s_{NN}} = 2.76$ TeV. *Phys. Rev. Lett.* **109**, 252302 (2012). [arXiv:1203.2436](#) [nucl-ex]
35. ALICE Collaboration, Centrality dependence of particle production in p–Pb collisions at $\sqrt{s_{NN}} = 5.02$ TeV. *Phys. Rev. C* **91**, 064905 (2015). [arXiv:1412.6828](#) [nucl-ex]
36. C. Patrignani, P. D. G. Others, Review of particle physics. *Chin. Phys. C* **40**, 100001 (2016)
37. ALICE Collaboration, Measurement of prompt J/ψ and beauty hadron production cross sections at mid-rapidity in pp collisions at $\sqrt{s} = 7$ TeV. *J. High Energy Phys.* **11**, 065 (2012). [arXiv:1205.5880](#) [hep-ex]
38. ALICE Collaboration, Inclusive, prompt and non-prompt J/ψ production at mid-rapidity in Pb–Pb collisions at $\sqrt{s_{NN}} = 2.76$ TeV. *J. High Energy Phys.* **07**, 051 (2015). [arXiv:1504.07151](#) [nucl-ex]
39. D. Lange, The EvtGen particle decay simulation package. *Nucl. Instrum. Methods A* **462**, 152 (2001)
40. LHCb Collaboration, Measurement of J/ψ production in pp collisions at $\sqrt{s} = 7$ TeV. *Eur. Phys. J. C* **71**, 1645 (2011). [arXiv:1103.0423](#) [hep-ex]
41. ALICE Collaboration, J/ψ polarization in pp collisions at $\sqrt{s} = 7$ TeV. *Phys. Rev. Lett.* **108**, 082001 (2012). [arXiv:1111.1630](#) [hep-ex]
42. CMS Collaboration, Measurement of the prompt J/ψ and $\psi(2S)$ polarizations in pp collisions at $\sqrt{s} = 7$ TeV. *Phys. Lett. B* **727**, 381 (2013). [arXiv:1307.6070](#) [hep-ex]
43. H. Fritzsche, Producing heavy quark flavors in hadronic collisions: a test of quantum chromodynamics. *Phys. Lett. B* **67**, 217 (1977)
44. F. Halzen, CVC for gluons and hadroproduction of quark flavors. *Phys. Lett. B* **69**, 105 (1977)
45. J. Albacete et al., Predictions for p + Pb collisions at $\sqrt{s_{NN}} = 5$ TeV. *Int. J. Mod. Phys. E* **22**, 1330007 (2013). [arXiv:1301.3395](#) [hep-ph]
46. K. Eskola, H. Paukkunen, C. Salgado, EPS09—a new generation of NLO and LO nuclear parton distribution functions. *J. High Energy Phys.* **04**, 065 (2009). [arXiv:0902.4154](#) [hep-ph]
47. T. Sjostrand, S. Mrenna, P. Z. Skands, PYTHIA 6.4 physics and manual. *J. High Energy Phys.* **05**, 026 (2006). [arXiv:hep-ph/0603175](#)
48. P.Z. Skands, Tuning Monte Carlo generators: the Perugia tunes. *Phys. Rev. D* **82**, 074018 (2010). [arXiv:1005.3457](#) [hep-ph]
49. X.-N. Wang, M. Gyulassy, Hijing: a Monte Carlo model for multiple jet production in pp, pA, and AA collisions. *Phys. Rev. D* **44**, 3501 (1991)
50. R. Brun, F. Carminati, S. Giani, GEANT detector description and simulation tool. CERN-W-5013 (1994)
51. E. Barberio, Z. Was, PHOTOS: a universal Monte Carlo for QED radiative corrections. Version 2.0. *Comput. Phys. Comm.* **79**, 291 (1994)
52. M. Cacciari, S. Frixione, N. Houdeau, M. Mangano, P. Nason, G. Ridolfi, Theoretical predictions for charm and bottom production at the LHC. *J. High Energy Phys.* **10**, 137 (2012). [arXiv:1205.6344](#) [hep-ph]
53. F. Bossu et al., Phenomenological interpolation of the inclusive J/ψ cross section to proton–proton collisions at 2.76 TeV and 5.5 TeV. [arXiv:1103.2394](#) [nucl-ex]
54. K. Eskola, P. Paakkinen, H. Paukkunen, C. Salgado, EPPS16: nuclear parton distributions with LHC data. *Eur. Phys. J. C* **77**, 163 (2017). [arXiv:1612.05741](#) [hep-ph]
55. K. Kovarik et al., nCTEQ15: global analysis of nuclear parton distributions with uncertainties in the CTEQ framework. *Phys. Rev. D* **93**, 085037 (2016)
56. A. Kusina, J.-P. Lansberg, I. Schienbein, H.-S. Shao, Gluon shadowing and antishadowing in heavy-flavor production at the LHC. [arXiv:1712.07024](#) [hep-ph]
57. CDF Collaboration, Measurement of the J/ψ meson and b-hadron production cross sections in $p\bar{p}$ collisions at $\sqrt{s} = 1960$ GeV. *Phys. Rev. D* **71**, 032001 (2005). [arXiv:hep-ex/0412071](#)
58. ATLAS Collaboration, Measurement of the differential cross-sections of inclusive, prompt and non-prompt J/ψ production in proton–proton collisions at $\sqrt{s} = 7$ TeV. *Nucl. Phys. B* **850**, 387 (2011). [arXiv:1104.3038](#) [hep-ex]
59. CMS Collaboration, Prompt and non-prompt J/ψ production in pp collisions at $\sqrt{s} = 7$ TeV. *Eur. Phys. J. C* **71**, 1575 (2011). [arXiv:1011.4193](#) [hep-ex]
60. ATLAS Collaboration, Measurement of the differential cross-sections of prompt and non-prompt production of J/ψ and $\psi(2S)$ in pp collisions at $\sqrt{s} = 7$ and 8 TeV with the ATLAS detector. *Eur. Phys. J. C* **76**, 283 (2016). [arXiv:1512.03657](#) [hep-ex]
61. P. Nadolsky, H.-L. Lai, Q.-H. Cao, J. Huston, J. Pumplin, D. Stump, W.-K. Tung, C.-P. Yuan, Implications of CTEQ global analysis for collider observables. *Phys. Rev. D* **78**, 013004 (2008). [arXiv:0802.0007](#) [hep-ph]
62. D. de Florian, R. Sassot, P. Zurita, M. Stratmann, Global analysis of nuclear parton distributions. *Phys. Rev. D* **85**, 074028 (2012). [arXiv:1112.6324](#) [hep-ph]
63. ALEPH Collaboration, Measurements of mean lifetime and branching fractions of b hadrons decaying to J/ψ . *Phys. Lett. B* **295**, 396 (1992)
64. L3 Collaboration, χ_c production in hadronic Z decays. *Phys. Lett. B* **317**, 467 (1993)
65. DELPHI Collaboration, J/ψ production in the hadronic decays of the Z. *Phys. Lett. B* **341**, 109 (1994)
66. R. Vogt, Cold nuclear matter effects on J/ψ and Υ production at the LHC. *Phys. Rev. C* **81**, 044903 (2010). [arXiv:1003.3497](#) [hep-ph]
67. F. Arleo, R. Kolevator, S. Peigne, M. Rostamova, Centrality and p_t dependence of J/ψ suppression in proton–nucleus collisions from parton energy loss. *J. High Energy Phys.* **05**, 155 (2013). [arXiv:1304.0901](#) [hep-ph]
68. E.G. Ferreira, F. Fleuret, J.P. Lansberg, A. Rakotozafindrabe, Impact of the nuclear modification of the gluon densities on J/ψ production in pPb collisions at $\sqrt{s_{NN}} = 5$ TeV. *Phys. Rev. C* **88**, 047901 (2013). [arXiv:1305.4569](#) [hep-ph]
69. H. Fujii, K. Watanabe, Heavy quark pair production in high energy pA collisions: quarkonium. *Nucl. Phys. A* **915**, 1 (2013). [arXiv:1304.2221](#) [hep-ph]

70. B. Ducloué, T. Lappi, H. Mäntysaar, Forward J/ψ production in proton-nucleus collisions at high energy. Phys. Rev. D **91**, 114005 (2015). [arXiv:1503.02789](https://arxiv.org/abs/1503.02789) [hep-ph]
71. G.T. Bodwin, E. Braaten, G.P. Lepage, Rigorous QCD analysis of inclusive annihilation and production of heavy quarkonium. Phys. Rev. D **51**, 1125 (1995). [arXiv:hep-ph/9407339](https://arxiv.org/abs/hep-ph/9407339) [hep-ph]
72. Y.-Q. Ma, R. Venugopalan, H.-F. Zhang, J/ψ production and suppression in high-energy proton–nucleus collisions. Phys. Rev. D **92**, 071901(R) (2015). [arXiv:1503.07772](https://arxiv.org/abs/1503.07772) [hep-ph]
73. E.G. Ferreira, Excited charmonium suppression in proton–nucleus collisions as a consequence of comovers. Phys. Lett. B **749**, 98 (2015). [arXiv:1411.0549](https://arxiv.org/abs/1411.0549) [hep-ph]

ALICE Collaboration

S. Acharya¹³⁹, F. T. Acosta²², D. Adamová⁹⁴, J. Adolphsson⁸¹, M. M. Aggarwal⁹⁸, G. Aglieri Rinella³⁶, M. Agnello³³, N. Agrawal⁴⁸, Z. Ahammed¹³⁹, S. U. Ahn⁷⁷, S. Aiola¹⁴⁴, A. Akindinov⁶⁴, M. Al-Turany¹⁰⁴, S. N. Alam¹³⁹, D. S. D. Albuquerque¹²⁰, D. Aleksandrov⁸⁸, B. Alessandro⁵⁸, R. Alfaro Molina⁷², Y. Ali¹⁶, A. Alici^{11,29,53}, A. Alkin³, J. Alme²⁴, T. Alt⁶⁹, L. Altenkamper²⁴, I. Altsybeev¹³⁸, C. Andrei⁴⁷, D. Andreou³⁶, H. A. Andrews¹⁰⁸, A. Andronic¹⁰⁴, M. Angeletti³⁶, V. Anguelov¹⁰², C. Anson¹⁷, T. Antičić¹⁰⁵, F. Antinori⁵⁶, P. Antonioli⁵³, N. Apadula⁸⁰, L. Aphecetche¹¹², H. Appelshäuser⁶⁹, S. Arcelli²⁹, R. Arnaldi⁵⁸, O. W. Arnold^{103,115}, I. C. Arsene²³, M. Arslandok¹⁰², B. Audurier¹¹², A. Augustinus³⁶, R. Averbeck¹⁰⁴, M. D. Azmi¹⁸, A. Badalà⁵⁵, Y. W. Baek^{60,76}, S. Bagnasco⁵⁸, R. Bailhache⁶⁹, R. Bala⁹⁹, A. Baldisseri¹³⁵, M. Ball⁴³, R. C. Baral^{66,86}, A. M. Barbano²⁸, R. Barbera³⁰, F. Barile⁵², L. Barioglio²⁸, G. G. Barnaföldi¹⁴³, L. S. Barnby⁹³, V. Barret¹³², P. Bartalini⁷, K. Barth³⁶, E. Bartsch⁶⁹, N. Bastid¹³², S. Basu¹⁴¹, G. Batigne¹¹², B. Batyunya⁷⁵, P. C. Batzing²³, J. L. Bazo Alba¹⁰⁹, I. G. Bearden⁸⁹, H. Beck¹⁰², C. Bedda⁶³, N. K. Behera⁶⁰, I. Belikov¹³⁴, F. Bellini^{29,36}, H. Bello Martinez², R. Bellwied¹²⁴, L. G. E. Beltran¹¹⁸, V. Belyaev⁹², G. Bencedi¹⁴³, S. Beole²⁸, A. Bercuci⁴⁷, Y. Berdnikov⁹⁶, D. Berenyi¹⁴³, R. A. Bertens¹²⁸, D. Berzano^{36,58}, L. Betev³⁶, P. P. Bhaduri¹³⁹, A. Bhasin⁹⁹, I. R. Bhat⁹⁹, B. Bhattacharjee⁴², J. Bhom¹¹⁶, A. Bianchi²⁸, L. Bianchi¹²⁴, N. Bianchi⁵¹, J. Bielčičk³⁸, J. Bielčičková⁹⁴, A. Bilandzic^{103,115}, G. Biro¹⁴³, R. Biswas⁴, S. Biswas⁴, J. T. Blair¹¹⁷, D. Blau⁸⁸, C. Blume⁶⁹, G. Boca¹³⁶, F. Bock³⁶, A. Bogdanov⁹², L. Boldizsár¹⁴³, M. Bombara³⁹, G. Bonomi¹³⁷, M. Bonora³⁶, H. Borel¹³⁵, A. Borissov^{20,102}, M. Borri¹²⁶, E. Botta²⁸, C. Bourjau⁸⁹, L. Bratrud⁶⁹, P. Braun-Munzinger¹⁰⁴, M. Bregant¹¹⁹, T. A. Broker⁶⁹, M. Broz³⁸, E. J. Brucken⁴⁴, E. Bruna⁵⁸, G. E. Bruno^{35,36}, D. Budnikov¹⁰⁶, H. Buesching⁶⁹, S. Bufalino³³, P. Buhler¹¹¹, P. Buncic³⁶, O. Busch¹³¹, Z. Buthelezi⁷³, J. B. Butt¹⁶, J. T. Buxton¹⁹, J. Cabala¹¹⁴, D. Caffarri^{36,90}, H. Caines¹⁴⁴, A. Caliva^{63,104}, E. Calvo Villar¹⁰⁹, R. S. Camacho², P. Camerini²⁷, A. A. Capon¹¹¹, F. Carena³⁶, W. Carena³⁶, F. Carnesecchi^{11,29}, J. Castillo Castellanos¹³⁵, A. J. Castro¹²⁸, E. A. R. Casula⁵⁴, C. Ceballos Sanchez⁹, S. Chandra¹³⁹, B. Chang¹²⁵, W. Chang⁷, S. Chapeland³⁶, M. Chartier¹²⁶, S. Chattopadhyay¹³⁹, S. Chattopadhyay¹⁰⁷, A. Chauvin^{103,115}, C. Cheshkov¹³³, B. Cheynis¹³³, V. Chibante Barroso³⁶, D. D. Chinellato¹²⁰, S. Cho⁶⁰, P. Chochula³⁶, S. Choudhury¹³⁹, T. Chowdhury¹³², P. Christakoglou⁹⁰, C. H. Christensen⁸⁹, P. Christiansen⁸¹, T. Chujo¹³¹, S. U. Chung²⁰, C. Cicalo⁵⁴, L. Cifarelli^{11,29}, F. Cindolo⁵³, J. Cleymans¹²³, F. Colamaria^{35,52}, D. Colella^{36,52,65}, A. Collu⁸⁰, M. Colocci²⁹, M. Concas^{58,b}, G. Conesa Balbastre⁷⁹, Z. Conesa del Valle⁶¹, J. G. Contreras³⁸, T. M. Cormier⁹⁵, Y. Corrales Morales⁵⁸, I. Cortés Maldonado², P. Cortese³⁴, M. R. Cosentino¹²¹, F. Costa³⁶, S. Costanza¹³⁶, J. Crkovská⁶¹, P. Crochet¹³², E. Cuautle⁷⁰, L. Cunqueiro^{95,142}, T. Dahms^{103,115}, A. Dainese⁵⁶, M. C. Danisch¹⁰², A. Danu⁶⁸, D. Das¹⁰⁷, I. Das¹⁰⁷, S. Das⁴, A. Dash⁸⁶, S. Dash⁴⁸, S. De⁴⁹, A. De Caro³², G. de Cataldo⁵², C. de Conti¹¹⁹, J. de Cuveland⁴⁰, A. De Falco²⁶, D. De Gruttola^{11,32}, N. De Marco⁵⁸, S. De Pasquale³², R. D. De Souza¹²⁰, H. F. Degenhardt¹¹⁹, A. Deisting^{102,104}, A. Deloff⁸⁵, S. Delsanto²⁸, C. Deplano⁹⁰, P. Dhankher⁴⁸, D. Di Bari³⁵, A. Di Mauro³⁶, B. Di Ruzza⁵⁶, R. A. Diaz⁹, T. Dietel¹²³, P. Dillenseger⁶⁹, Y. Ding⁷, R. Divià³⁶, Ø. Djuvsland²⁴, A. Dobrin³⁶, D. Domenicis Gimenez¹¹⁹, B. Dönigus⁶⁹, O. Dordic²³, L. V. R. Doremalen⁶³, A. K. Dubey¹³⁹, A. Dubla¹⁰⁴, L. Ducroux¹³³, S. Dudi⁹⁸, A. K. Duggal⁹⁸, M. Dukhishyam⁸⁶, P. Dupieux¹³², R. J. Ehlers¹⁴⁴, D. Elia⁵², E. Endress¹⁰⁹, H. Engel⁷⁴, E. Epple¹⁴⁴, B. Erazmus¹¹², F. Erhardt⁹⁷, M. R. Ersdal²⁴, B. Espagnon⁶¹, G. Eulisse³⁶, J. Eum²⁰, D. Evans¹⁰⁸, S. Evdokimov⁹¹, L. Fabbietti^{103,115}, M. Faggin³¹, J. Faivre⁷⁹, A. Fantoni⁵¹, M. Fasel⁹⁵, L. Feldkamp¹⁴², A. Feliciello⁵⁸, G. Feofilov¹³⁸, A. Fernández Téllez², A. Ferretti²⁸, A. Festanti^{31,36}, V. J. G. Feuillard^{132,135}, J. Figiel¹¹⁶, M. A. S. Figueredo¹¹⁹, S. Filchagin¹⁰⁶, D. Finogeev⁶², F. M. Fionda^{24,26}, M. Floris³⁶, S. Foertsch⁷³, P. Foka¹⁰⁴, S. Fokin⁸⁸, E. Fragiaco⁵⁹, A. Francescon³⁶, A. Francisco¹¹², U. Frankenfeld¹⁰⁴, G. G. Fronze²⁸, U. Fuchs³⁶, C. Furget⁷⁹, A. Furs⁶², M. Fusco Girard³², J. J. Gaardhøje⁸⁹, M. Gagliardi²⁸, A. M. Gago¹⁰⁹, K. Gajdosova⁸⁹, M. Gallio²⁸, C. D. Galvan¹¹⁸, P. Ganoti⁸⁴, C. Garabatos¹⁰⁴, E. Garcia-Solis¹², K. Garg³⁰, C. Gargiulo³⁶, P. Gasik^{103,115}, E. F. Gauger¹¹⁷, M. B. Gay Ducati⁷¹, M. Germain¹¹², J. Ghosh¹⁰⁷, P. Ghosh¹³⁹, S. K. Ghosh⁴, P. Gianotti⁵¹, P. Giubellino^{58,104}, P. Giubilato³¹, P. Glässel¹⁰², D. M. Gómez Coral⁷², A. Gomez Ramirez⁷⁴, P. González-Zamora², S. Gorbunov⁴⁰, L. Görlich¹¹⁶, S. Gotovac¹²⁷, V. Grabski⁷², L. K. Graczykowski¹⁴⁰, K. L. Graham¹⁰⁸

L. Greiner⁸⁰, A. Grelli⁶³, C. Grigoras³⁶, V. Grigoriev⁹², A. Grigoryan¹, S. Grigoryan⁷⁵, J. M. Gronefeld¹⁰⁴, F. Grosa³³, J. F. Grosse-Oetringhaus³⁶, R. Grosso¹⁰⁴, R. Guernane⁷⁹, B. Guerzoni²⁹, M. Guittiere¹¹², K. Gulbrandsen⁸⁹, T. Gunji¹³⁰, A. Gupta⁹⁹, R. Gupta⁹⁹, I. B. Guzman², R. Haake³⁶, M. K. Habib¹⁰⁴, C. Hadjidakis⁶¹, H. Hamagaki⁸², G. Hamar¹⁴³, J. C. Hamon¹³⁴, M. R. Haque⁶³, J. W. Harris¹⁴⁴, A. Harton¹², H. Hassan⁷⁹, D. Hatzifotiadou^{11,53}, S. Hayashi¹³⁰, S. T. Heckel⁶⁹, E. Hellbär⁶⁹, H. Helstrup³⁷, A. Herghelegiu⁴⁷, E. G. Hernandez², G. Herrera Corral¹⁰, F. Herrmann¹⁴², K. F. Hetland³⁷, H. Hillemanns³⁶, C. Hills¹²⁶, B. Hippolyte¹³⁴, B. Hohlweger¹⁰³, D. Horak³⁸, S. Hornung¹⁰⁴, R. Hosokawa^{79,131}, P. Hristov³⁶, C. Hughes¹²⁸, P. Huhn⁶⁹, T. J. Humanic¹⁹, H. Hushnud¹⁰⁷, N. Hussain⁴², T. Hussain¹⁸, D. Hutter⁴⁰, D. S. Hwang²¹, J. P. Iddon¹²⁶, S. A. Iga Buitron⁷⁰, R. Ilkaev¹⁰⁶, M. Inaba¹³¹, M. Ippolitov^{88,92}, M. S. Islam¹⁰⁷, M. Ivanov¹⁰⁴, V. Ivanov⁹⁶, V. Izucheev⁹¹, B. Jacak⁸⁰, N. Jacazio²⁹, P. M. Jacobs⁸⁰, M. B. Jadhav⁴⁸, S. Jadlovská¹¹⁴, J. Jadlovsky¹¹⁴, S. Jaelani⁶³, C. Jahnke^{115,119}, M. J. Jakubowska¹⁴⁰, M. A. Janik¹⁴⁰, P. H. S. Y. Jayarathna¹²⁴, C. Jena⁸⁶, M. Jercic⁹⁷, R. T. Jimenez Bustamante¹⁰⁴, P. G. Jones¹⁰⁸, A. Jusko¹⁰⁸, P. Kalinak⁶⁵, A. Kalweit³⁶, J. H. Kang¹⁴⁵, V. Kaplin⁹², S. Kar¹³⁹, A. Karasu Uysal⁷⁸, O. Karavichev⁶², T. Karavicheva⁶², L. Karayan^{102,104}, P. Karczmarczyk³⁶, E. Karpechev⁶², U. Kbschull⁷⁴, R. Keidel⁴⁶, D. L. D. Keijdener⁶³, M. Keil³⁶, B. Ketzer⁴³, Z. Khabanova⁹⁰, S. Khan¹⁸, S. A. Khan¹³⁹, A. Khanzadeev⁹⁶, Y. Kharlov⁹¹, A. Khatun¹⁸, A. Khuntia⁴⁹, M. M. Kielbowicz¹¹⁶, B. Kileng³⁷, B. Kim¹³¹, D. Kim¹⁴⁵, D. J. Kim¹²⁵, E. J. Kim¹⁴, H. Kim¹⁴⁵, J. S. Kim⁴¹, J. Kim¹⁰², M. Kim⁶⁰, S. Kim²¹, T. Kim¹⁴⁵, S. Kirsch⁴⁰, I. Kisel⁴⁰, S. Kiselev⁶⁴, A. Kisiel¹⁴⁰, G. Kiss¹⁴³, J. L. Klay⁶, C. Klein⁶⁹, J. Klein^{36,58}, C. Klein-Bösing¹⁴², S. Klewin¹⁰², A. Kluge³⁶, M. L. Knichel^{36,102}, A. G. Knospe¹²⁴, C. Kobdaj¹¹³, M. Kofarago¹⁴³, M. K. Köhler¹⁰², T. Kollegger¹⁰⁴, V. Kondratiev¹³⁸, N. Kondratyeva⁹², E. Kondratyuk⁹¹, A. Konevskikh⁶², M. Konyushikhin¹⁴¹, O. Kovalenko⁸⁵, V. Kovalenko¹³⁸, M. Kowalski¹¹⁶, I. Králik⁶⁵, A. Kravčáková³⁹, L. Kreis¹⁰⁴, M. Krivda^{65,108}, F. Krizek⁹⁴, M. Krüger⁶⁹, E. Kryshen⁹⁶, M. Krzewicki⁴⁰, A. M. Kubera¹⁹, V. Kučera⁹⁴, C. Kuhn¹³⁴, P. G. Kuijser⁹⁰, J. Kumar⁴⁸, L. Kumar⁹⁸, S. Kumar⁴⁸, S. Kundu⁸⁶, P. Kurashvili⁸⁵, A. Kurepin⁶², A. B. Kurepin⁶², A. Kuryakin¹⁰⁶, S. Kushpil⁹⁴, M. J. Kweon⁶⁰, Y. Kwon¹⁴⁵, S. L. La Pointe⁴⁰, P. La Rocca³⁰, C. Lagana Fernandes¹¹⁹, Y. S. Lai⁸⁰, I. Lakomov³⁶, R. Langoy¹²², K. Lapidus¹⁴⁴, C. Lara⁷⁴, A. Lardeux²³, P. Larionov⁵¹, A. Lattuca²⁸, E. Laudi³⁶, R. Lavicka³⁸, R. Lea²⁷, L. Leardini¹⁰², S. Lee¹⁴⁵, F. Lehas⁹⁰, S. Lehner¹¹¹, J. Lehrbach⁴⁰, R. C. Lemmon⁹³, E. Leogrande⁶³, I. León Monzón¹¹⁸, P. Lévai¹⁴³, X. Li¹³, X. L. Li⁷, J. Lien¹²², R. Lietava¹⁰⁸, B. Lim²⁰, S. Lindal²³, V. Lindenstruth⁴⁰, S. W. Lindsay¹²⁶, C. Lippmann¹⁰⁴, M. A. Lisa¹⁹, V. Litichevskiy⁴⁴, A. Liu⁸⁰, H. M. Ljunggren⁸¹, W. J. Llope¹⁴¹, D. F. Lodato⁶³, V. Loginov⁹², C. Loizides^{80,95}, P. Loncar¹²⁷, X. Lopez¹³², E. López Torres⁹, A. Lowe¹⁴³, P. Luettig⁶⁹, J. R. Luhder¹⁴², M. Lunardon³¹, G. Luparello^{27,59}, M. Lupi³⁶, A. Maevskaya⁶², M. Mager³⁶, S. M. Mahmood²³, A. Maire¹³⁴, R. D. Majka¹⁴⁴, M. Malaev⁹⁶, L. Malinina^{75,c}, D. Mal'Kevich⁶⁴, P. Malzacher¹⁰⁴, A. Mamonov¹⁰⁶, V. Manko⁸⁸, F. Manso¹³², V. Manzari⁵², Y. Mao⁷, M. Marchisone^{73,129,133}, J. Mareš⁶⁷, G. V. Margagliotti²⁷, A. Margotti⁵³, J. Margutti⁶³, A. Marín¹⁰⁴, C. Markert¹¹⁷, M. Marquard⁶⁹, N. A. Martin¹⁰⁴, P. Martinengo³⁶, J. A. L. Martinez⁷⁴, M. I. Martínez², G. Martínez García¹¹², M. Martinez Pedreira³⁶, S. Masciocchi¹⁰⁴, M. Maserà²⁸, A. Masoni⁵⁴, L. Massacrier⁶¹, E. Masson¹¹², A. Mastroserio⁵², A. M. Mathis^{103,115}, P. F. T. Matuoka¹¹⁹, A. Matyja¹²⁸, C. Mayer¹¹⁶, M. Mazzilli³⁵, M. A. Mazzoni⁵⁷, F. Meddi²⁵, Y. Melikyan⁹², A. Menchaca-Rocha⁷², J. Mercado Pérez¹⁰², M. Meres¹⁵, S. Mhlanga¹²³, Y. Miake¹³¹, L. Micheletti²⁸, M. M. Mieskolainen⁴⁴, D. L. Mihaylov¹⁰³, K. Mikhaylov^{64,75}, A. Mischke⁶³, D. Miśkowiec¹⁰⁴, J. Mitra¹³⁹, C. M. Mitu⁶⁸, N. Mohammadi^{36,63}, A. P. Mohanty⁶³, B. Mohanty⁸⁶, M. Mohisin Khan^{18,d}, D. A. Moreira De Godoy¹⁴², L. A. P. Moreno², S. Moretto³¹, A. Morreale¹¹², A. Morsch³⁶, V. Muccifora⁵¹, E. Mudnic¹²⁷, D. Mühlheim¹⁴², S. Muhuri¹³⁹, M. Mukherjee⁴, J. D. Mulligan¹⁴⁴, M. G. Munhoz¹¹⁹, K. Munning⁴³, M. I. A. Munoz⁸⁰, R. H. Munzer⁶⁹, H. Murakami¹³⁰, S. Murray⁷³, L. Musa³⁶, J. Musinsky⁶⁵, C. J. Myers¹²⁴, J. W. Myrcha¹⁴⁰, B. Naik⁴⁸, R. Nair⁸⁵, B. K. Nandi⁴⁸, R. Nania^{11,53}, E. Nappi⁵², A. Narayan⁴⁸, M. U. Naru¹⁶, H. Natal da Luz¹¹⁹, C. Nattrass¹²⁸, S. R. Navarro², K. Nayak⁸⁶, R. Nayak⁴⁸, T. K. Nayak¹³⁹, S. Nazarenko¹⁰⁶, R. A. Negrao De Oliveira^{36,69}, L. Nellen⁷⁰, S. V. Nesbo³⁷, G. Neskovic⁴⁰, F. Ng¹²⁴, M. Nicassio¹⁰⁴, J. Niedziela^{36,140}, B. S. Nielsen⁸⁹, S. Nikolaev⁸⁸, S. Nikulin⁸⁸, V. Nikulin⁹⁶, F. Noferini^{11,53}, P. Nomokonov⁷⁵, G. Nooren⁶³, J. C. C. Noris², J. Norman^{79,126}, A. Nyanin⁸⁸, J. Nystrand²⁴, H. Oeschler^{20,102,a}, H. Oh¹⁴⁵, A. Ohlson¹⁰², L. Olah¹⁴³, J. Oleniacz¹⁴⁰, A. C. Oliveira Da Silva¹¹⁹, M. H. Oliver¹⁴⁴, J. Onderwaater¹⁰⁴, C. Oppedisano⁵⁸, R. Orava⁴⁴, M. Oravec¹¹⁴, A. Ortiz Velasquez⁷⁰, A. Oskarsson⁸¹, J. Otwinowski¹¹⁶, K. Oyama⁸², Y. Pachmayer¹⁰², V. Pacic⁸⁹, D. Pagano¹³⁷, G. Paic⁷⁰, P. Palni⁷, J. Pan¹⁴¹, A. K. Pandey⁴⁸, S. Panebianco¹³⁵, V. Papikyan¹, P. Pareek⁴⁹, J. Park⁶⁰, S. Parmar⁹⁸, A. Passfeld¹⁴², S. P. Pathak¹²⁴, R. N. Patra¹³⁹, B. Paul⁵⁸, H. Pei⁷, T. Peitzmann⁶³, X. Peng⁷, L. G. Pereira⁷¹, H. Pereira Da Costa¹³⁵, D. Peresunko^{88,92}, E. Perez Lezama⁶⁹, V. Peskov⁶⁹, Y. Pestov⁵, V. Petráček³⁸, M. Petrovici⁴⁷, C. Petta³⁰, R. P. Pezzi⁷¹, S. Piano⁵⁹, M. Pikna¹⁵, P. Pillot¹¹², L. O. D. L. Pimentel⁸⁹, O. Pinazza^{36,53}, L. Pinsky¹²⁴, S. Pisano⁵¹, D. B. Piyarathna¹²⁴, M. Płoskoń⁸⁰, M. Planinic⁹⁷, F. Pliquet⁶⁹, J. Pluta¹⁴⁰, S. Pochybova¹⁴³, P. L. M. Podesta-Lerma¹¹⁸, M. G. Poghosyan⁹⁵, B. Polichtchouk⁹¹, N. Poljak⁹⁷, W. Poonsawat¹¹³, A. Pop⁴⁷, H. Popenborg¹⁴², S. Porteboeuf-Houssais¹³², V. Pozdniakov⁷⁵

S. K. Prasad⁴, R. Preghenella⁵³, F. Prino⁵⁸, C. A. Pruneau¹⁴¹, I. Pshenichnov⁶², M. Puccio²⁸, V. Punin¹⁰⁶, J. Putschke¹⁴¹, S. Raha⁴, S. Rajput⁹⁹, J. Rak¹²⁵, A. Rakotozafindrabe¹³⁵, L. Ramello³⁴, F. Rami¹³⁴, D. B. Rana¹²⁴, R. Raniwala¹⁰⁰, S. Raniwala¹⁰⁰, S. S. Räsänen⁴⁴, B. T. Rascanu⁶⁹, D. Rathee⁹⁸, V. Ratza⁴³, I. Ravasenga³³, K. F. Read^{95,128}, K. Redlich^{85,e}, A. Rehman²⁴, P. Reichelt⁶⁹, F. Reidt³⁶, X. Ren⁷, R. Renfordt⁶⁹, A. Reshetin⁶², K. Reygiers¹⁰², V. Riabov⁹⁶, T. Richert^{63,81}, M. Richter²³, P. Riedler³⁶, W. Riegler³⁶, F. Riggi³⁰, C. Ristea⁶⁸, M. Rodríguez Cahuantzi², K. Røed²³, R. Rogalev⁹¹, E. Rogochaya⁷⁵, D. Rohr³⁶, D. Röhrich²⁴, P.S. Rokita¹⁴⁰, F. Ronchetti⁵¹, E. D. Rosas⁷⁰, K. Roslon¹⁴⁰, P. Rosnet¹³², A. Rossi^{31,56}, A. Rotondi¹³⁶, F. Roukoutakis⁸⁴, C. Roy¹³⁴, P. Roy¹⁰⁷, O. V. Rueda⁷⁰, R. Rui²⁷, B. Rumyantsev⁷⁵, A. Rustamov⁸⁷, E. Ryabinkin⁸⁸, Y. Ryabov⁹⁶, A. Rybicki¹¹⁶, S. Saarinen⁴⁴, S. Sadhu¹³⁹, S. Sadovsky⁹¹, K. Šafařík³⁶, S. K. Saha¹³⁹, B. Sahoo⁴⁸, P. Sahoo⁴⁹, R. Sahoo⁴⁹, S. Sahoo⁶⁶, P. K. Sahu⁶⁶, J. Saini¹³⁹, S. Sakai¹³¹, M. A. Saleh¹⁴¹, S. Sambyal⁹⁹, V. Samsonov^{92,96}, A. Sandoval⁷², A. Sarkar⁷³, D. Sarkar¹³⁹, N. Sarkar¹³⁹, P. Sarma⁴², M. H. P. Sas⁶³, E. Scapparone⁵³, F. Scarlassara³¹, B. Schaefer⁹⁵, H. S. Scheid⁶⁹, C. Schiaua⁴⁷, R. Schicker¹⁰², C. Schmidt¹⁰⁴, H. R. Schmidt¹⁰¹, M. O. Schmidt¹⁰², M. Schmidt¹⁰¹, N. V. Schmidt^{69,95}, J. Schukraft³⁶, Y. Schutz^{36,134}, K. Schwarz¹⁰⁴, K. Schweda¹⁰⁴, G. Scioli²⁹, E. Scomparin⁵⁸, M. Šefčík³⁹, J. E. Seger¹⁷, Y. Sekiguchi¹³⁰, D. Sekihata⁴⁵, I. Selyuzhenkov^{92,104}, K. Senosi⁷³, S. Senyukov¹³⁴, E. Serradilla⁷², P. Sett⁴⁸, A. Sevcenco⁶⁸, A. Shabanov⁶², A. Shabetai¹¹², R. Shahoyan³⁶, W. Shaikh¹⁰⁷, A. Shangaraev⁹¹, A. Sharma⁹⁸, A. Sharma⁹⁹, N. Sharma⁹⁸, A. I. Sheikh¹³⁹, K. Shigaki⁴⁵, M. Shimomura⁸³, S. Shirinkin⁶⁴, Q. Shou^{7,110}, K. Shtejer²⁸, Y. Sibiriak⁸⁸, S. Siddhanta⁵⁴, K. M. Sielewicz³⁶, T. Siemiarczuk⁸⁵, S. Silaeva⁸⁸, D. Silvermyr⁸¹, G. Simatovic^{90,97}, G. Simonetti^{36,103}, R. Singaraju¹³⁹, R. Singh⁸⁶, V. Singhal¹³⁹, T. Sinha¹⁰⁷, B. Sitar¹⁵, M. Sitta³⁴, T. B. Skaali²³, M. Slupecki¹²⁵, N. Smirnov¹⁴⁴, R. J. M. Snellings⁶³, T. W. Snellman¹²⁵, J. Song²⁰, F. Soramel³¹, S. Sorensen¹²⁸, F. Sozzi¹⁰⁴, I. Sputowska¹¹⁶, J. Stachel¹⁰², I. Stan⁶⁸, P. Stankus⁹⁵, E. Stenlund⁸¹, D. Stocco¹¹², M. M. Storetvedt³⁷, P. Strmen¹⁵, A. A. P. Suaide¹¹⁹, T. Sugitate⁴⁵, C. Suire⁶¹, M. Suleymanov¹⁶, M. Suljic²⁷, R. Sultanov⁶⁴, M. Šumbera⁹⁴, S. Sumowidagdo⁵⁰, K. Suzuki¹¹¹, S. Swain⁶⁶, A. Szabo¹⁵, I. Szarka¹⁵, U. Tabassam¹⁶, J. Takahashi¹²⁰, G. J. Tambave²⁴, N. Tanaka¹³¹, M. Tarhini^{61,112}, M. Tariq¹⁸, M. G. Tarzila⁴⁷, A. Tauro³⁶, G. Tejada Muñoz², A. Telesca³⁶, K. Terasaki¹³⁰, C. Terrevoli³¹, B. Teyssier¹³³, D. Thakur⁴⁹, S. Thakur¹³⁹, D. Thomas¹¹⁷, F. Thoresen⁸⁹, R. Tieulent¹³³, A. Tikhonov⁶², A. R. Timmins¹²⁴, A. Toia⁶⁹, N. Topilskaya⁶², M. Toppi⁵¹, S. R. Torres¹¹⁸, S. Tripathy⁴⁹, S. Trogolo²⁸, G. Trombetta³⁵, L. Tropp³⁹, V. Trubnikov³, W. H. Trzaska¹²⁵, T. P. Trzcinski¹⁴⁰, B. A. Trzeciak⁶³, T. Tsuji¹³⁰, A. Tumkin¹⁰⁶, R. Turrisi⁵⁶, T. S. Tveter²³, K. Ullaland²⁴, E. N. Umaka¹²⁴, A. Uras¹³³, G. L. Usai²⁶, A. Utrobicic⁹⁷, M. Vala¹¹⁴, J. Van Der Maarel⁶³, J. W. Van Hoorne³⁶, M. van Leeuwen⁶³, T. Vanat⁹⁴, P. Vande Vyvre³⁶, D. Varga¹⁴³, A. Vargas², M. Vargyas¹²⁵, R. Varma⁴⁸, M. Vasileiou⁸⁴, A. Vasiliev⁸⁸, A. Vauthier⁷⁹, O. Vázquez Doce^{103,115}, V. Vechernin¹³⁸, A. M. Veen⁶³, A. Velure²⁴, E. Vercellin²⁸, S. Vergara Limón², L. Vermunt⁶³, R. Vernet⁸, R. Vértesi¹⁴³, L. Vickovic¹²⁷, J. Viinikainen¹²⁵, Z. Vilakazi¹²⁹, O. Villalobos Baillie¹⁰⁸, A. Villatoro Tello², A. Vinogradov⁸⁸, L. Vinogradov¹³⁸, T. Virgili³², V. Vislavicius⁸¹, A. Vodopyanov⁷⁵, M. A. Völkl¹⁰¹, K. Voloshin⁶⁴, S. A. Voloshin¹⁴¹, G. Volpe³⁵, B. von Haller³⁶, I. Vorobyev^{103,115}, D. Voscek¹¹⁴, D. Vranic^{36,104}, J. Vrláková³⁹, B. Wagner²⁴, H. Wang⁶³, M. Wang⁷, Y. Watanabe^{130,131}, M. Weber¹¹¹, S. G. Weber¹⁰⁴, A. Wegrzynek³⁶, D. F. Weiser¹⁰², S. C. Wenzel³⁶, J. P. Wessels¹⁴², U. Westerhoff¹⁴², A. M. Whitehead¹²³, J. Wiechula⁶⁹, J. Wikne²³, G. Wilk⁸⁵, J. Wilkinson⁵³, G. A. Willems^{36,142}, M. C. S. Williams⁵³, E. Willsher¹⁰⁸, B. Windelband¹⁰², W. E. Witt¹²⁸, R. Xu⁷, S. Yalcin⁷⁸, K. Yamakawa⁴⁵, P. Yang⁷, S. Yano⁴⁵, Z. Yin⁷, H. Yokoyama^{79,131}, I.-K. Yoo²⁰, J. H. Yoon⁶⁰, E. Yun²⁰, V. Yurchenko³, V. Zaccolo⁵⁸, A. Zaman¹⁶, C. Zampolli³⁶, H. J. C. Zanoli¹¹⁹, N. Zardoshti¹⁰⁸, A. Zarochentsev¹³⁸, P. Závada⁶⁷, N. Zaviyalov¹⁰⁶, H. Zbroszczyk¹⁴⁰, M. Zhalov⁹⁶, H. Zhang⁷, X. Zhang⁷, Y. Zhang⁷, Z. Zhang^{7,132}, C. Zhao²³, N. Zhigareva⁶⁴, D. Zhou⁷, Y. Zhou⁸⁹, Z. Zhou²⁴, H. Zhu⁷, J. Zhu⁷, Y. Zhu⁷, A. Zichichi^{11,29}, M.B. Zimmermann³⁶, G. Zinovjev³, J. Zmeskal¹¹¹, S. Zou⁷

¹ A.I. Alikhanyan National Science Laboratory (Yerevan Physics Institute) Foundation, Yerevan, Armenia

² Benemérita Universidad Autónoma de Puebla, Puebla, Mexico

³ Bogolyubov Institute for Theoretical Physics, National Academy of Sciences of Ukraine, Kiev, Ukraine

⁴ Department of Physics and Centre for Astroparticle Physics and Space Science (CAPSS), Bose Institute, , Kolkata, India

⁵ Budker Institute for Nuclear Physics, Novosibirsk, Russia

⁶ California Polytechnic State University, San Luis Obispo, CA, USA

⁷ Central China Normal University, Wuhan, China

⁸ Centre de Calcul de l'IN2P3, Villeurbanne, Lyon, France

⁹ Centro de Aplicaciones Tecnológicas y Desarrollo Nuclear (CEADEN), Havana, Cuba

¹⁰ Centro de Investigación y de Estudios Avanzados (CINVESTAV), Mexico City and Mérida, Mexico

- 11 Centro Fermi - Museo Storico della Fisica e Centro Studi e Ricerche “Enrico Fermi”, Rome, Italy
- 12 Chicago State University, Chicago, IL, USA
- 13 China Institute of Atomic Energy, Beijing, China
- 14 Chonbuk National University, Jeonju, Republic of Korea
- 15 Comenius University Bratislava, Faculty of Mathematics, Physics and Informatics, Bratislava, Slovakia
- 16 COMSATS Institute of Information Technology (CIIT), Islamabad, Pakistan
- 17 Creighton University, Omaha, NE, USA
- 18 Department of Physics, Aligarh Muslim University, Aligarh, India
- 19 Department of Physics, Ohio State University, Columbus, OH, USA
- 20 Department of Physics, Pusan National University, Pusan, Republic of Korea
- 21 Department of Physics, Sejong University, Seoul, Republic of Korea
- 22 Department of Physics, University of California, Berkeley, CA, USA
- 23 Department of Physics, University of Oslo, Oslo, Norway
- 24 Department of Physics and Technology, University of Bergen, Bergen, Norway
- 25 Dipartimento di Fisica dell’Università ‘La Sapienza’ and Sezione INFN, Rome, Italy
- 26 Dipartimento di Fisica dell’Università and Sezione INFN, Cagliari, Italy
- 27 Dipartimento di Fisica dell’Università and Sezione INFN, Trieste, Italy
- 28 Dipartimento di Fisica dell’Università and Sezione INFN, Turin, Italy
- 29 Dipartimento di Fisica e Astronomia dell’Università and Sezione INFN, Bologna, Italy
- 30 Dipartimento di Fisica e Astronomia dell’Università and Sezione INFN, Catania, Italy
- 31 Dipartimento di Fisica e Astronomia dell’Università and Sezione INFN, Padua, Italy
- 32 Dipartimento di Fisica ‘E.R. Caianiello’ dell’Università and Gruppo Collegato INFN, Salerno, Italy
- 33 Dipartimento DISAT del Politecnico and Sezione INFN, Turin, Italy
- 34 Dipartimento di Scienze e Innovazione Tecnologica dell’Università del Piemonte Orientale and INFN Sezione di Torino, Alessandria, Italy
- 35 Dipartimento Interateneo di Fisica ‘M. Merlin’ and Sezione INFN, Bari, Italy
- 36 European Organization for Nuclear Research (CERN), Geneva, Switzerland
- 37 Faculty of Engineering and Science, Western Norway University of Applied Sciences, Bergen, Norway
- 38 Faculty of Nuclear Sciences and Physical Engineering, Czech Technical University in Prague, Prague, Czech Republic
- 39 Faculty of Science, P.J. Šafárik University, Košice, Slovakia
- 40 Frankfurt Institute for Advanced Studies, Johann Wolfgang Goethe-Universität Frankfurt, Frankfurt, Germany
- 41 Gangneung-Wonju National University, Gangneung, Republic of Korea
- 42 Department of Physics, Gauhati University, Guwahati, India
- 43 Helmholtz-Institut für Strahlen- und Kernphysik, Rheinische Friedrich-Wilhelms-Universität Bonn, Bonn, Germany
- 44 Helsinki Institute of Physics (HIP), Helsinki, Finland
- 45 Hiroshima University, Hiroshima, Japan
- 46 Hochschule Worms, Zentrum für Technologietransfer und Telekommunikation (ZTT), Worms, Germany
- 47 Horia Hulubei National Institute of Physics and Nuclear Engineering, Bucharest, Romania
- 48 Indian Institute of Technology Bombay (IIT), Mumbai, India
- 49 Indian Institute of Technology Indore, Indore, India
- 50 Indonesian Institute of Sciences, Jakarta, Indonesia
- 51 INFN, Laboratori Nazionali di Frascati, Frascati, Italy
- 52 INFN, Sezione di Bari, Bari, Italy
- 53 INFN, Sezione di Bologna, Bologna, Italy
- 54 INFN, Sezione di Cagliari, Cagliari, Italy
- 55 INFN, Sezione di Catania, Catania, Italy
- 56 INFN, Sezione di Padova, Padua, Italy
- 57 INFN, Sezione di Roma, Rome, Italy
- 58 INFN, Sezione di Torino, Turin, Italy
- 59 INFN, Sezione di Trieste, Trieste, Italy
- 60 Inha University, Incheon, Republic of Korea

- 61 Institut de Physique Nucléaire d'Orsay (IPNO), Institut National de Physique Nucléaire et de Physique des Particules (IN2P3/CNRS), Université de Paris-Sud, Université Paris-Saclay, Orsay, France
- 62 Institute for Nuclear Research, Academy of Sciences, Moscow, Russia
- 63 Institute for Subatomic Physics, Utrecht University/Nikhef, Utrecht, The Netherlands
- 64 Institute for Theoretical and Experimental Physics, Moscow, Russia
- 65 Institute of Experimental Physics, Slovak Academy of Sciences, Košice, Slovakia
- 66 Institute of Physics, Bhubaneswar, India
- 67 Institute of Physics of the Czech Academy of Sciences, Prague, Czech Republic
- 68 Institute of Space Science (ISS), Bucharest, Romania
- 69 Institut für Kernphysik, Johann Wolfgang Goethe-Universität Frankfurt, Frankfurt, Germany
- 70 Instituto de Ciencias Nucleares, Universidad Nacional Autónoma de México, Mexico City, Mexico
- 71 Instituto de Física, Universidade Federal do Rio Grande do Sul (UFRGS), Porto Alegre, Brazil
- 72 Instituto de Física, Universidad Nacional Autónoma de México, Mexico City, Mexico
- 73 iThemba LABS, National Research Foundation, Somerset West, South Africa
- 74 Johann-Wolfgang-Goethe Universität Frankfurt Institut für Informatik, Fachbereich Informatik und Mathematik, Frankfurt, Germany
- 75 Joint Institute for Nuclear Research (JINR), Dubna, Russia
- 76 Konkuk University, Seoul, Republic of Korea
- 77 Korea Institute of Science and Technology Information, Daejeon, Republic of Korea
- 78 KTO Karatay University, Konya, Turkey
- 79 Laboratoire de Physique Subatomique et de Cosmologie, Université Grenoble-Alpes, CNRS-IN2P3, Grenoble, France
- 80 Lawrence Berkeley National Laboratory, Berkeley, CA, USA
- 81 Division of Particle Physics, Lund University Department of Physics, Lund, Sweden
- 82 Nagasaki Institute of Applied Science, Nagasaki, Japan
- 83 Nara Women's University (NWU), Nara, Japan
- 84 Department of Physics, School of Science, National and Kapodistrian University of Athens, Athens, Greece
- 85 National Centre for Nuclear Research, Warsaw, Poland
- 86 National Institute of Science Education and Research, HBNI, Jatni, India
- 87 National Nuclear Research Center, Baku, Azerbaijan
- 88 National Research Centre Kurchatov Institute, Moscow, Russia
- 89 Niels Bohr Institute, University of Copenhagen, Copenhagen, Denmark
- 90 Nikhef, National institute for subatomic physics, Amsterdam, The Netherlands
- 91 NRC Kurchatov Institute IHEP, Protvino, Russia
- 92 NRNU Moscow Engineering Physics Institute, Moscow, Russia
- 93 Nuclear Physics Group, STFC Daresbury Laboratory, Daresbury, UK
- 94 Nuclear Physics Institute of the Czech Academy of Sciences, Řež u Prahy, Czech Republic
- 95 Oak Ridge National Laboratory, Oak Ridge, TN, USA
- 96 Petersburg Nuclear Physics Institute, Gatchina, Russia
- 97 Physics department, Faculty of science, University of Zagreb, Zagreb, Croatia
- 98 Physics Department, Panjab University, Chandigarh, India
- 99 Physics Department, University of Jammu, Jammu, India
- 100 Physics Department, University of Rajasthan, Jaipur, India
- 101 Physikalisches Institut, Eberhard-Karls-Universität Tübingen, Tübingen, Germany
- 102 Physikalisches Institut, Ruprecht-Karls-Universität Heidelberg, Heidelberg, Germany
- 103 Physik Department, Technische Universität München, Munich, Germany
- 104 Research Division and ExtreMe Matter Institute EMMI, GSI Helmholtzzentrum für Schwerionenforschung GmbH, Darmstadt, Germany
- 105 Rudjer Bošković Institute, Zagreb, Croatia
- 106 Russian Federal Nuclear Center (VNIIEF), Sarov, Russia
- 107 Saha Institute of Nuclear Physics, Kolkata, India
- 108 School of Physics and Astronomy, University of Birmingham, Birmingham, UK
- 109 Sección Física, Departamento de Ciencias, Pontificia Universidad Católica del Perú, Lima, Peru

- 110 Shanghai Institute of Applied Physics, Shanghai, China
111 Stefan Meyer Institut für Subatomare Physik (SMI), Vienna, Austria
112 SUBATECH, IMT Atlantique, Université de Nantes, CNRS-IN2P3, Nantes, France
113 Suranaree University of Technology, Nakhon Ratchasima, Thailand
114 Technical University of Košice, Košice, Slovakia
115 Technische Universität München, Excellence Cluster 'Universe', Munich, Germany
116 The Henryk Niewodniczanski Institute of Nuclear Physics, Polish Academy of Sciences, Cracow, Poland
117 The University of Texas at Austin, Austin, TX, USA
118 Universidad Autónoma de Sinaloa, Culiacán, Mexico
119 Universidade de São Paulo (USP), São Paulo, Brazil
120 Universidade Estadual de Campinas (UNICAMP), Campinas, Brazil
121 Universidade Federal do ABC, Santo Andre, Brazil
122 University College of Southeast Norway, Tonsberg, Norway
123 University of Cape Town, Cape Town, South Africa
124 University of Houston, Houston, TX, USA
125 University of Jyväskylä, Jyväskylä, Finland
126 University of Liverpool, Liverpool, UK
127 Faculty of Electrical Engineering, Mechanical Engineering and Naval Architecture, University of Split, Split, Croatia
128 University of Tennessee, Knoxville, TN, USA
129 University of the Witwatersrand, Johannesburg, South Africa
130 University of Tokyo, Tokyo, Japan
131 University of Tsukuba, Tsukuba, Japan
132 Université Clermont Auvergne, CNRS/IN2P3, LPC, Clermont-Ferrand, France
133 Université de Lyon, Université Lyon 1, CNRS/IN2P3, IPN-Lyon, Villeurbanne, Lyon, France
134 Université de Strasbourg, CNRS, IPHC UMR 7178, 67000 Strasbourg, France
135 Département de Physique Nucléaire (DPhN), Université Paris-Saclay Centre d'Études de Saclay (CEA), IRFU, Saclay, France
136 Università degli Studi di Pavia, Pavia, Italy
137 Università di Brescia, Brescia, Italy
138 V. Fock Institute for Physics, St. Petersburg State University, St. Petersburg, Russia
139 Variable Energy Cyclotron Centre, Kolkata, India
140 Warsaw University of Technology, Warsaw, Poland
141 Wayne State University, Detroit, MI, USA
142 Westfälische Wilhelms-Universität Münster, Institut für Kernphysik, Münster, Germany
143 Wigner Research Centre for Physics, Hungarian Academy of Sciences, Budapest, Hungary
144 Yale University, New Haven, CT, USA
145 Yonsei University, Seoul, Republic of Korea

^a Deceased

^b Dipartimento DET del Politecnico di Torino, Turin, Italy

^c M.V. Lomonosov Moscow State University, D.V. Skobeltsyn Institute of Nuclear, Physics, Moscow, Russia

^d Department of Applied Physics, Aligarh Muslim University, Aligarh, India

^e Institute of Theoretical Physics, University of Wrocław, Poland